In presenting the dissertation as a partial fulfillment of the requirements for an advanced degree from the Georgia Institute of Technology, I agree that the Library of the Institute shall make it available for inspection and circulation in accordance with its regulations governing materials of this type. I agree that permission to copy from, or to publish from, this dissertation may be granted by the professor under whose direction it was written, or, in his absence, by the Dean of the Graduate Division when such copying or publication is solely for scholarly purposes and does not involve potential financial gain. It is understood that any copying from, or publication of, this dissertation which involves potential financial gain will not be allowed without written permission.

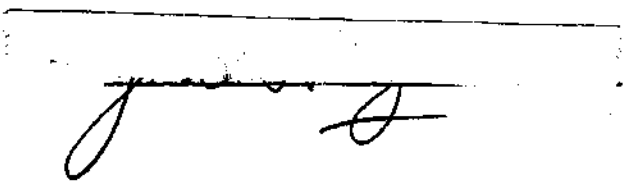

3/17/65
b

INVESTIGATION OF THE HEAT TRANSFER FROM AN ISOTHERMAL CYLINDER EXPOSED TO CROSSFLOW OF A WATER-AIR SPRAY

A THESIS

Presented to

The Faculty of the Graduate Division

by

Jeffrey William Hodgson

In Partial Fulfillment

of the Requirements for the Degree

Doctor of Philosophy

in the School of Mechanical Engineering

Georgia Institute of Technology

July, 1967

INVESTIGATION OF THE HEAT TRANSFER FROM AN

ISOTHERMAL CYLINDER EXPOSED TO CROSSFLOW OF A WATER-AIR SPRAY

Approved:

Chairman

Date approved by Chairman: 7/12/67

ACKNOWLEDGMENTS

The author would like to acknowledge here a few of the many people who have been instrumental in helping him to attain this long sought-after goal: Dr. J. E. Sunderland, his thesis advisor, whose efforts on the author's behalf will always be remembered, and who gave through his actions countless examples of personal and professional ethics of the highest order; Dr. T. W. Jackson, who served as the author's master's thesis advisor, as a member of his Ph.D. thesis committee, and as a continual source of encouragement and contagious optimism; Professor A. C. Bruce, who taught two of the most interesting courses the author took, and who made many helpful suggestions and constructive criticisms while serving on the Ph.D. thesis committee; Dr. W. W. Graham and Dr. W. M. Williams, who served on the author's final examining committee; Messrs. W. C. Thomas and R. T. Saterbak who performed a vast majority of the design and construction of the wind tunnel; Mr. J. G. Doyal, Technician, whose rare ability to cooperate with student researchers makes him a most valuable member of the staff; and Dr. K. G. Picha, who encouraged the author to enter graduate school.

Finally, the author would like to thank his wife, Peggie; his parents; and his parents-in-law; whose patience, encouragement, and love made possible his graduate studies.

The research upon which this thesis is based was supported by National Science Foundation Grant No. GK-766. The author would like to express his appreciation to the Foundation for these funds and for the

N. S. F. Co-operative Graduate Fellowship awarded to him for 1963-1966.

TABLE OF CONTENTS

LIST OF TABLES

LIST OF ILLUSTRATIONS

SUMMARY

An analytical and experimental program was conducted to investigate the heat transfer which occurs when a heated, isothermal, horizontal, circular cylinder is exposed to a vertical crossflow consisting of a water-in-air spray.

The analytical investigation applies integral forms of the continuity, momentum, and energy equations to the liquid film formed on the cylinder. Third order polynomial expressions for the velocity and temperature profiles in the film are assumed. Under the additional assumptions of incompressible flow, negligible evaporation from the film, and no deflection of the droplets as they approach the cylinder; a closed form expression for the local Nusselt number is obtained as a function of the air free stream Reynolds number and the water-to-air mass flow ratio. The analysis is valid for the leading 160 degrees of the cylinder.

A closed loop wind tunnel was constructed to provide a vertical two-component fluid stream (water was sprayed into the air above the test section). A three-inch diameter test cylinder with 12 30-degree segments (each equipped with its own electrical heater) was placed in the air stream. Experimental values of the local Nusselt number around the cylinder were obtained for air Reynolds numbers of 30,000, 75,000 and 118,000. Water-to-air mass flow ratios of from 1 to 6 per cent were used.

Good agreement is indicated between the theoretical and experi-

mental Nusselt numbers. This study may clarify conflicting results reported by two other investigators by showing good agreement with one of them. Increases in the local Nusselt numbers for two-component flow are on the order of 30 times those experienced in single-component (air) flow at the same Reynolds numbers.

It is recommended that future work in the field of spray heat transfer deal with the practical implementation of the results of this study.

NOMENCLATURE

English Letters		Typical Units
a, b, c, d	coefficients in the polynomial velocity profile	dimensionless
a_t, b_t, c_t, d_t	coefficients in the polynomial temperature profile	dimensionless
c_{pl}	specific heat of the liquid	Btu/lb_m-°F
f	polynomial temperature distribution in the film = θ/θ_δ	dimensionless
f_t	polynomial temperature distribution in the film = θ/θ_o	dimensionless
f_v	polynomial velocity distribution in the film	dimensionless
g	local acceleration of gravity	ft/sec^2
h_a	local single-component (air) heat transfer coefficient	Btu/ft^2-°F-hr
h_{fg}	enthalpy of evaporation of the liquid	Btu/lb_m
h_L	local two-component heat transfer coefficient	Btu/ft^2-°F-hr
h_δ	local convective heat transfer coefficient between the film and the air flowing over it	Btu/ft^2-°F-hr
k_a	thermal conductivity of air	Btu/hr-ft-°F
k_l	thermal conductivity of the liquid	Btu/hr-ft-°F
$\dot{m}''_{evap}$	local evaporation rate from the film	lb_m/ft^2-hr
$\dot{m}_l$	mass flow rate of liquid in the free stream per unit area	lb_m/ft^2-sec

English Letters		Typical Units
$\dot{m}_r$	liquid-to-air mass flow ratio in the free stream	dimensionless
p	local pressure in the film	lb_f/ft^2
p_e	local external (air) pressure	lb_f/ft^2
r	radial co-ordinate measured from the center of the cylinder	ft
D	cylinder diameter	ft
F_ϕ	ϕ-component of the body force	lb_f/lb_m
R	cylinder radius	ft
T	temperature	°F
T_o	cylinder temperature	°F
T_r	reference temperature for liquid enthalpy	°F
T_δ	temperature at the film-air interface	°F
T_∞	free stream temperature of the droplets	°F
TAU	Blasius shear polynomial	dimensionless
U_ϕ	ϕ-velocity in the film	ft/sec
U_δ	ϕ-velocity at the film-air interface	ft/sec
U_∞	free stream velocity upstream from the cylinder	ft/sec
Greek Letters		
α_l	thermal diffusivity of the liquid	ft^2/hr
δ	film thickness	ft

Greek Letters		Typical Units
$\bar{\delta}$	normalized film thickness	dimensionless
η	dimensionless co-ordinate normal to the cylinder	dimensionless
θ	$T - T_\infty$	°F
θ_o	$T_o - T_\infty$	°F
θ_δ	$T_\delta - T_\infty$	°F
μ_a	dynamic viscosity of the air	$lb_m/ft\text{-}sec$
μ_l	dynamic viscosity of the liquid	$lb_m/ft\text{-}sec$
ρ_a	density of the air	lb_m/ft^3
ρ_l	density of the liquid	lb_m/ft^3
$\bar{\rho}$	ratio of the density of the liquid to that air	dimensionless
τ_e	external shear stress acting on the film due to the air flow	lb_f/ft^2
τ_l	shear stress that would exist in the film if the velocity profile were linear	lb_f/ft^2
τ_o	shear stress acting on the film at the cylinder surface	lb_f/ft^2
ϕ	angular co-ordinate measured from the leading stagnation point	radians

Dimensionless Groups	
Nu_δ	local Nusselt number between the air and the film = $h_\delta D/k_a$
Nu_A	local single-component (air) Nusselt number = $h_a D/k_a$

Dimensionless Groups

Nu_L	local two-component Nusselt number = $h_L D/k_1$
Pe_1	Peclet number for the liquid = $Re_1 Pr_1$
Pr_1	Prandtl number of the liquid
Re	free stream Reynolds number based on the free stream velocity, U_∞, the cylinder diameter, D, and the kinematic viscosity of air
Re_1	same as Re except the kinematic viscosity of the liquid is used

CHAPTER I

INTRODUCTION

Definition of the Problem

In the field of heat transfer it is not uncommon for a thermal energy exchange to occur in which a two-component, two-phase fluid is involved. A common example of the above occurs whenever an aircraft flies through rain or when a spray of water is directed onto a heat exchanger to improve its performance. In order to gain insight into the mechanisms of heat transfer under these conditions it would be helpful to investigate both analytically and experimentally the heat transfer involving a body of simple geometry when it is exposed to a two-component, two-phase fluid stream. This study is therefore concerned with the problem of predicting analytically and measuring experimentally the heat transfer that occurs from a heated cylinder when it is exposed to a two-component, two-phase (spray) stream.

Background

The possibilities of increasing the heat transfer from an air cooled heat exchanger by adding water droplets to the air stream were reported in 1961 by Elperin (1)* who conducted experiments on tube bundles exposed to a water-air spray. Interest grew quickly and the initial investigation in this country was reported in 1964 by Acrivos

---

*Numbers in parentheses refer to the Literature Cited, page 108.

et al. (2) in which the heat transfer from a single vertical cylinder exposed to a spray was measured. From direct observations Acrivos and his associates concluded that four different models might be applicable for the study of problems of this type. The first model postulates that the liquid droplets impinge on the cylinder, evaporate immediately, and no liquid film builds up on the surface. Another model considers the case when the droplets bounce off the cylinder. The third and fourth models postulate the existence of a liquid film on the surface--the difference between these two models being that one of them considers evaporation from the film to be significant, whereas evaporation is neglected in the other. Experimental observations (2) verified the existence of the first model only under extreme conditions of cylinder temperatures and droplet flow rates. The bouncing droplet model was also observed, but in conjunction with a liquid film on the cylinder. The most prevalent (and the most easily obtained) models were the liquid film models without droplet bouncing.

Results obtained by Acrivos et al. showed an increase in overall two-component (spray) heat transfer of from 2.5 to 9.0 times that which occurred with no spray. These investigators attempted to predict analytically the heat transfer under the conditions of the non-evaporating film, but could only show that their simplifying assumptions were invalid. They concluded ". . . that a more detailed analysis is required."

Further experimental work was performed by Hoelscher (3) in 1965. He concluded, although not without reservations, that the back side of the cylinder contributes only slightly to the total heat transfer. He did not attempt an analytical study.

Tifford (4) presented an analytical solution which applied for flat plates. He neglected the local pressure gradients and gravity forces. In addition Tifford also assumed that the liquid film was laminar, that linear velocity and temperature profiles existed in the film, and that the velocity and temperature at the free surface of the film were constants. The last two assumptions would seem to be poor, particularly for the case of a circular cylinder. Tifford discusses this somewhat in his presentation, but refers only to flat plate applications.

As a follow-up to Hoelscher's work, Takahara (5) modified the heated vertical cylinder used by Hoelscher and took more care to define the temperature difference upon which the heat transfer coefficient was based. In both Acrivos' work and Hoelscher's work the air being blown over the cylinder was at a different temperature than the spray water introduced. This coupled with the fact that the air was not saturated (relative humidity less than 100 per cent) led to some uncertainty concerning the temperature of both the droplets and the air as they intercepted the cylinder. Takahara saturated the air before the spray was added to it and also controlled the temperature of the spray in order to make it the same as the air temperature. It is felt that these precautions taken by Takahara lend more credence to his experimental results than can be given to either Acrivos or Hoelscher. Takahara did not attempt an analytical investigation.

An analytical study of the spray-cooled cylinder was reported by Goldstein et al. (6) in 1966. In his work Goldstein considered the differential forms of the transport equations as applied to the liquid

film formed on the cylinder. His solution is by numerical techniques, however, which limits the usefulness of his results. The theoretical results compare favorably with experimental data of Acrivos, et al. (2).

The most recent (1966) study of heat transfer from a cylinder to a spray was performed by Smith (7). Smith presented an analytical study which agreed quite well with his experimental data despite the fact that his final equation contains an error (see Appendix B). His results, however, are not in agreement with those obtained by Takahara and there is no apparent reason for the discrepancy--other than the existence of a systematic error in either (or both) of their programs. Smith found it impossible to saturate the air entering his wind tunnel and therefore had to perform tests with air having a low relative humidity (45 per cent). As a result, his droplets were subjected to evaporation before they reached the cylinder.

An analytical and experimental investigation of the heat transfer from a wedge exposed to a spray was conducted by Thomas (8) using the same wind tunnel as the present study. Thomas reported very good agreement between his analytical and experimental results.

The present study was conducted in cooperation with Mr. R. T. Saterbak who performed a major portion of the experimental work. Saterbak's thesis (9) contains the bulk of the experimental data obtained during the study.

As indicated, the literature contains four sources of experimental data and two analytical studies covering the problem of heat transfer from a spray-cooled cylinder. The author believes, however, that the existing data contain inconsistencies and perhaps inaccuracies which

should be resolved through a separate, independent program of research. The basis for these allegations is as follows:

Acrivos (2) and his associates had difficulty with their apparatus because water dripped from the horizontal wind tunnel walls onto their vertical cylinder. They also took no precautions in defining the temperature difference upon which they based their heat transfer coefficients, and as a result their study is valuable only as a source of qualitative data. It cannot be used for any quantitative information. Hoelscher (3), as stated earlier, concluded that the heat transfer from the downstream side of his cylinder was negligible. Actually he observed "negative" heat transfer coefficients in this area--the cause being blamed on heat conduction from the front half of the cylinder to the back half via the cement holding his heaters in place. Hoelscher also failed to carefully define his temperature difference and his results are, therefore, subject to the same limitations as those of Acrivos.

The work of Takahara (5) is subject to question mainly because of the very large discrepancies between it and the latest study by Smith (7). Takahara used the same equipment as Hoelscher, and although he carefully defined his temperature difference, the results showed no heat transfer from the back of the cylinder, but very large heat transfer from the front of the cylinder. One explanation for this is that Takahara experienced the same difficulty as Hoelscher--namely, heat conduction from the front heaters to the back heaters.

The work by Smith is subject to criticism because of the lack of control over the relative humidity of the air entering the test section. The humidity becomes another variable to consider in his program along

with the uncertainty concerning the droplet temperatures after exposure to the dry air.

In the experimental part of this study the air humidity was eliminated as a variable by saturating the air prior to the injection of water, and all precautions necessary to eliminate the effects of conduction within the cylinder were taken. By reducing the number of variables to a minimum, it was believed that the experimental program would yield significant insight into the mechanism by which the energy transfer occurs. It was anticipated that the results of this study would also serve to resolve the differences that exist between the results of Takahara and Smith.

As mentioned earlier, Goldstein's analysis necessitates an involved computer solution of his equations. Smith's analysis results in a closed form expression for the heat transfer coefficients, but considers only linear velocity and temperature profiles in the film and gives no indication as to how the equations were solved. One purpose of this study was to obtain a closed form solution for the heat transfer coefficients while allowing non-linear velocity and temperature profiles.

Purpose of the Research

The objectives of the research program upon which this thesis is based are:

1. To develop analytically a means of predicting the heat transfer from an isothermal circular cylinder exposed to a crossflow of a water-air spray. This analysis will show the influence of the free-stream Reynolds number, temperature difference between the spray and the

cylinder, and water-to-air mass flow ratio.

2. To compare the results obtained from the analytical study with experimental measurements of heat transfer around the cylinder.

CHAPTER II

THEORETICAL ANALYSIS

General

In the analysis of a problem involving spray-cooled surfaces it is essential that the flow regime under consideration be carefully specified. In the case of the present investigation in which an air-spray mixture is directed onto a heated circular cylinder, the most prevalent condition observed experimentally is the one which results in the formation of a continuous liquid film on the front half of the cylinder. The resultant increase in the heat transfer coefficient (over single-component gas flow) may be explained by the formation of this liquid "boundary layer" which replaces the gas boundary layer adjacent to the solid surface. The higher thermal conductivity (approximately 25 times higher) and the much higher heat capacity per unit volume (approximately 4,000 times higher) of water over air, result in an improved heat transfer situation when the liquid film exists.

When the flow is incompressible, evaporation negligible, and all properties (except pressure and temperature) are constants, then the momentum and energy equations as applied to the film are not coupled. It is therefore possible to solve the continuity and momentum equations (for the film thickness and the velocity distribution in the film) and substitute the results into the energy equation. This procedure is employed in the following sections.

The analytical technique selected for this study involves the use of the integral forms of the continuity, momentum, and energy equations as applied to the liquid film. As was pointed out earlier, Goldstein (6) considered the differential forms of the continuity, momentum, and energy equations and was faced with an involved numerical solution. In the past the integral technique has proven to be an excellent tool for the investigation of many problems of the boundary layer type. The approach is generally credited to von Karman and in fact it is often referred to as the von Karman integral technique. The validity of the integral technique was established by Pohlhausen (10) in 1921 when he applied it to an analysis of the laminar boundary layer on a cylinder in crossflow. Other examples of successful applications of integral equations include the analysis of transpiration cooling by Mouradian and Sunderland (11), the prediction of free convection heat transfer from a horizontal cylinder by Dyer (12), and a study of stagnation point ablation by Roberts (13).

The physical model used in the present work is shown in Figure 1. The control volume selected to aid the analysis is shown in Figure 2. The assumptions used in arriving at the governing integral equations are as follows:

1. An isothermal, horizontal, circular cylinder is exposed to a vertical crossflow of a water-air spray.

2. The flow is steady.

3. All physical properties remain constant due to the small pressure and temperature variations expected.

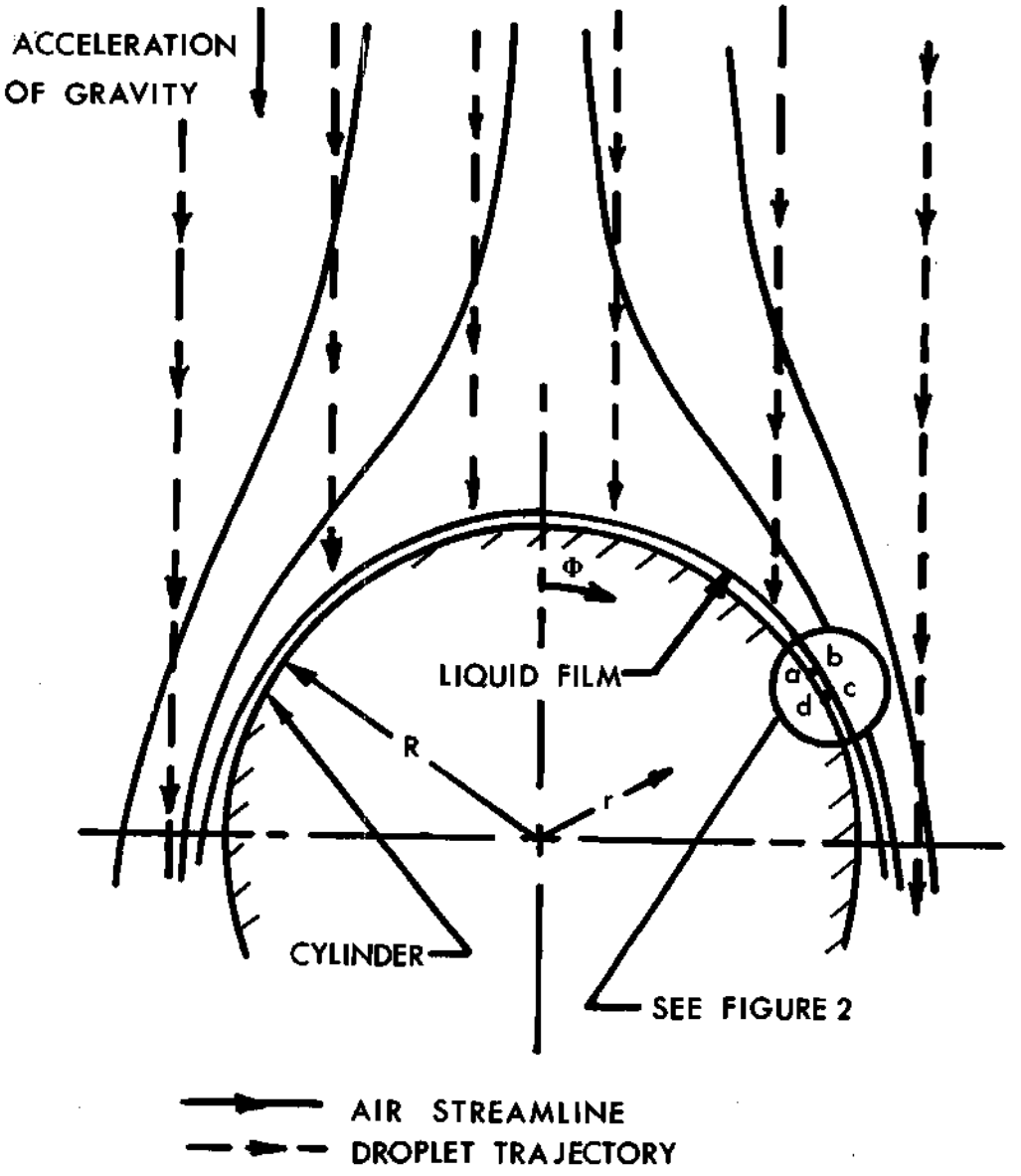

Figure 1. Physical Flow Model

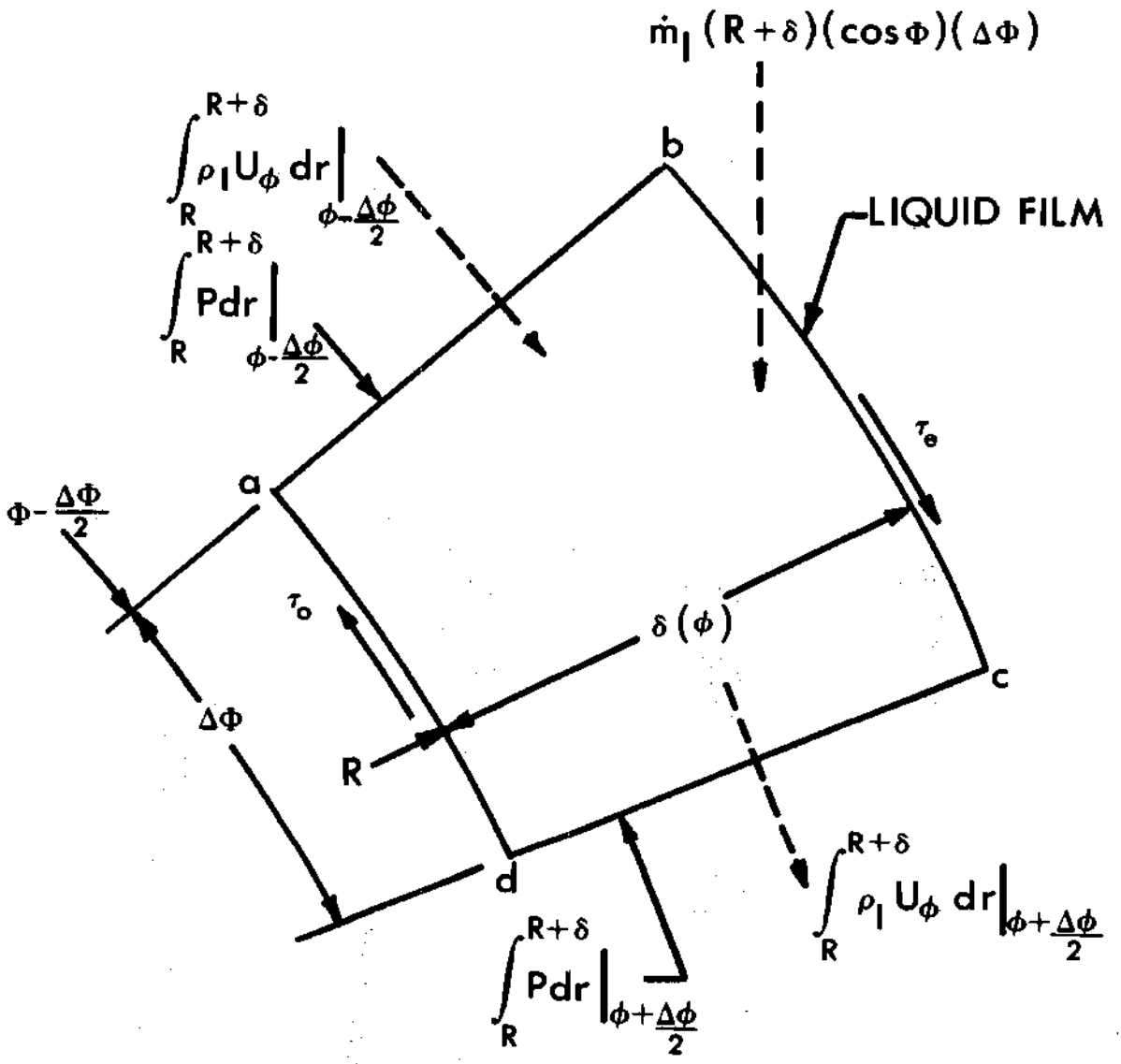

Figure 2. Control Volume abcd Showing Forces and Mass Fluxes

4. The water droplets are uniformly distributed throughout the air stream as it approaches the cylinder.

5. The droplets and the air ahead of the cylinder have the same velocity (see Chapter IV).

6. The droplets continue in straight paths unaffected by the air flow around the cylinder (see Appendix A).

7. The presence of droplets in the air stream does not affect the potential air flow around the cylinder (see Appendix A).

8. A liquid film is formed on the cylinder.

9. The liquid film is laminar. This assumption is made because the film moves slowly and is very thin.

10. The droplets are captured by the film causing only minor local disturbances which are rapidly damped out.

11. Evaporation from the film is negligible. This assumption is made because the air flowing over the cylinder will be saturated and the temperature of the cylinder will not be sufficient to cause a significant driving force for evaporation (see Appendix B).

12. Conduction in the ϕ-direction is negligible as in the case of most boundary layer type flows (see Appendix C).

13. The shear stress and the heat transfer coefficient between the edge of the film and the air are the same as they would be for the air flowing over the dry cylinder.

14. There is no viscous dissipation because the velocities are low.

15. Kinetic and potential energy changes are negligible.

Continuity Equation

The conservation of mass as applied to the liquid film states that the rate at which liquid flows past a radial section of the film is equal to the amount of liquid in droplet form which intercepted the cylinder prior to that section. Stated mathematically:

$$\int_{R}^{R+\delta} \rho_l U_\phi dr = \dot{m}_l R \sin\phi$$

where R is the radius of the cylinder, δ is the liquid film thickness, r is the radial co-ordinate, ρ_l is the density of the liquid in the film, U_ϕ is the ϕ-velocity in the film, ϕ is the angular co-ordinate measured from the forward stagnation point, and $\dot{m}_l$ is the droplet mass flow rate per unit area in the freestream. This same equation is obtained if one considers the control volume a-b-c-d in Figure 2 and performs a mass balance on it. The continuity equation contains two unknowns in the form of the film thickness, δ, and the velocity profile U_ϕ. Note that whenever evaporation becomes very significant, the above equation is not valid as it does not include any mass loss due to evaporation from the film.

Because water can be considered to be incompressible, the density term may be taken out of the integral and the resulting continuity equation is:

$$\int_{R}^{R+\delta} U_\phi \, dr = \frac{\dot{m}_l R \sin\phi}{\rho_l} \qquad (1)$$

Momentum Equation

The momentum equation is obtained by considering the forces acting on the control volume a-b-c-d of Figure 2 and setting the sum of these forces equal to the net momentum efflux from the control volume. Both the forces and the momentum are taken in the ϕ-direction only. Stated more precisely:

$$\sum (\text{Forces})_{\phi\text{-direction}} = (\text{Momentum rate out})_{\phi\text{-direction}} - (\text{momentum rate in})_{\phi\text{-direction}} \qquad (2)$$

Letting F_{ab} designate the force acting in the positive ϕ-direction on the ab face of the control volume,

$$F_{ab} = \left[\int_R^{R+\delta} p\, dr\right]_{\phi-\frac{\Delta\phi}{2}} \cos\left(\frac{\Delta\phi}{2}\right) \simeq \left\{\left[\int_R^{R+\delta} p\, dr\right]_{\phi} - \left[\frac{d}{d\phi}\int_R^{R+\delta} p\, dr\right]_{\phi}\left(\frac{\Delta\phi}{2}\right)\right\} \cos\left(\frac{\Delta\phi}{2}\right)$$

$$F_{bc} = \tau_e(R+\delta)\Delta\phi + p_e\left[\delta_{\phi+\frac{\Delta\phi}{2}} - \delta_{\phi-\frac{\Delta\phi}{2}}\right] \simeq \tau_e R\Delta\phi + p_e\left(\frac{d\delta}{d\phi}\right)\Delta\phi$$

$$F_{cd} = -\left[\int_R^{R+\delta} p\, dr\right]_{\phi+\frac{\Delta\phi}{2}} \cos\left(\frac{\Delta\phi}{2}\right) \simeq -\left\{\left[\int_R^{R+\delta} p\, dr\right]_{\phi} + \left[\frac{d}{d\phi}\int_R^{R+\delta} p\, dr\right]_{\phi}\left(\frac{\Delta\phi}{2}\right)\right\} \cos\left(\frac{\Delta\phi}{2}\right)$$

$$F_{ad} = -\tau_o R(\Delta\phi) \qquad \text{and} \qquad F_{body} = F_\phi \rho_1 \delta R(\Delta\phi).$$

Thus,

$$\sum (\text{Forces})_{\phi\text{-direction}} = F_{ab} + F_{bc} + F_{cd} + F_{ad} + F_{body} \tag{2a}$$

$$= \left\{ - \frac{d}{d\phi} \int_R^{R+\delta} p \, dr \cos\left(\frac{\Delta\phi}{2}\right) + (\tau_e - \tau_o)R + p_e\left(\frac{d\delta}{d\phi}\right) + F_\phi \rho_1 \delta R \right\} \Delta\phi$$

The momentum fluxes into the control volume in the ϕ-direction are:

$$\text{The momentum flux in a-b} = \left[\int_R^{R+\delta} \rho_1 U_\phi^{\,2} \, dr \right]_{\phi - \frac{\Delta\phi}{2}} \cos\left(\frac{\Delta\phi}{2}\right)$$

$$\tilde{=} \left\{ \left[\int_R^{R+\delta} \rho_1 U_\phi^{\,2} \, dr \right]_{\phi} - \left[\frac{d}{d\phi} \int_R^{R+\delta} \rho_1 U_\phi^{\,2} \, dr \right]_{\phi} \frac{\Delta\phi}{2} \right\} \cos\left(\frac{\Delta\phi}{2}\right)$$

$$\text{The momentum flux in b-c} = \dot{m}_1 U_\infty (R+\delta)\sin\phi\cos\phi(\Delta\phi) \tilde{=} \dot{m}_1 U_\infty R \sin\phi\cos\phi(\Delta\phi)$$

$$\text{The momentum flux out c-d} = \left[\int_R^{R+\delta} \rho_1 U_\phi^{\,2} \, dr \right]_{\phi + \frac{\Delta\phi}{2}} \cos\left(\frac{\Delta\phi}{2}\right)$$

$$\simeq \left\{ \left[\int_R^{R+\delta} \rho_1 U_\phi^{\,2}\, dr \right]_\phi + \left[\frac{d}{d\phi} \int_R^{R+\delta} \rho_1 U_\phi^{\,2}\, dr \right]_\phi \frac{\Delta\phi}{2} \right\} \cos\left(\frac{\Delta\phi}{2}\right)$$

Thus, the momentum rate out in the ϕ-direction minus the momentum rate in for the ϕ-direction is:

$$\left\{ \frac{d}{d\phi} \left[\int_R^{R+\delta} \rho_1 U_\phi^{\,2}\, dr \right] \cos\left(\frac{\Delta\phi}{2}\right) - \dot{m}_1 U_\infty R \sin\phi\cos\phi \right\} \Delta\phi \qquad (2b)$$

Substituting Equations (2a) and (2b) into Equation (2) yields (after dividing by $\Delta\phi$):

$$- \frac{d}{d\phi} \int_R^{R+\delta} p\, dr \cos\frac{\Delta\phi}{2} + (\tau_e - \tau_o)R + p_e\left(\frac{d\delta}{d\phi}\right) + F_\phi \rho_1 \delta R =$$

$$\frac{d}{d\phi} \int_R^{R+\delta} \rho_1 U_\phi^{\,2}\, dr \cos\frac{\Delta\phi}{2} - \dot{m}_1 U_\infty R \sin\phi\cos\phi$$

Taking the limit as $\Delta\phi$ goes to zero (and therefore $\cos\frac{\Delta\phi}{2}$ goes to one) and assuming that the external pressure field is impressed on the film so that $p = p_e$, there results:

$$- \frac{d}{d\phi}(p_e\, \delta) + (\tau_e + \tau_o)R + p_e \frac{d\delta}{d\phi} + F_\phi \rho_1 \delta R = \frac{d}{d\phi} \int_R^{R+\delta} \rho_1 U_\phi^{\,2}\, dr - \dot{m}_1 U_\infty R \sin\phi\cos\phi.$$

Introducing the variable η, which is a non-dimensional co-ordinate normal to the cylinder surface $\left(\eta = \frac{r - R}{\delta}\right)$, and the variable $\bar{\delta} = \frac{\delta}{R}$, which is a non-dimensional film thickness, there is obtained (after dividing the momentum equation by $\rho_a U_\infty^2 R$)

$$- \bar{\delta} \frac{1}{\rho_a U_\infty^2} \frac{dp}{d\phi} + \frac{\tau_e - \tau_o}{\rho_a U_\infty^2} + \frac{F_\phi}{U_\infty^2} \frac{R}{\rho_a} \frac{\rho_l}{\rho_a} \bar{\delta} = \frac{\rho_l}{\rho_a} \frac{d}{d\phi} \left[\bar{\delta} \int_0^1 \left(\frac{U_\phi}{U_\infty}\right)^2 d\eta \right] - \frac{\dot{m}_l}{\rho_a U_\infty} \sin\phi\cos\phi.$$

Since $\rho_a U_\infty$ represents the mass flow rate of air per unit area, the ratio of $\dot{m}_l$ to $\rho_a U_\infty$ is a measure of the droplet concentration in the air stream when the velocity of the air is the same as the droplets. This mass flow ratio is designated as $\dot{m}_r$. The final form of the ϕ-momentum equation is:

$$\bar{\rho} \frac{d}{d\phi} \left[\bar{\delta} \int_0^1 \left(\frac{U_\phi}{U_\infty}\right)^2 d\eta \right] + \bar{\delta} \frac{1}{\rho_a U_\infty^2} \frac{dp}{d\phi} + \frac{\tau_o - \tau_e}{\rho_a U_\infty^2} - \frac{F_\phi}{U_\infty^2} \frac{R}{\bar{\rho}} \bar{\delta} \qquad (3)$$

$$- \dot{m}_r \sin\phi\cos\phi = 0.$$

The terms represent (from left to right)

1. The film inertia.
2. The external force due to the pressure gradient.
3. The net force due to the difference between the external shear (produced by the air flow) and the drag experienced by the film at the cylinder surface.
4. The body force acting in the ϕ-direction.

5. The momentum addition due to the impact of the droplets as they enter the film.

In view of the very low film velocities observed (on the order of 1 ft/sec) by Acrivos (2), Hoelscher (3), and Smith (7) the film inertia term should be negligible compared to the other terms. The body force term is also felt to be small (later on it will be possible to verify this assumption). With both of these terms discarded, the momentum equation becomes:

$$\bar{\delta}\,\frac{1}{\rho_a U_\infty^{\,2}}\,\frac{dp}{d\phi} + \frac{\tau_o - \tau_e}{\rho_a U_\infty^{\,2}} - \dot{m}_r \sin\phi\cos\phi = 0 \qquad (4)$$

Solution of the Hydrodynamic Problem

The continuity and momentum equations specify the hydrodynamics involved in the liquid film behavior. In order to solve these equations for the film thickness, δ, and the velocity profile in the film, U_ϕ, it is necessary to assume some form for the velocity profile. In this study the velocity profile was assigned the form of a polynomial of third degree following the approach of Mouradian (11):

$$U_\phi = U_\delta(\phi) f_v(\phi,\eta)$$

where $U_\delta(\phi)$ is the velocity at the edge of the film, and $f_v(\phi,\eta)$ is a polynomial in η of the form:

$$f_v(\phi,\eta) = a(\phi) + b(\phi)\eta + c(\phi)\eta^2 + d(\phi)\eta^3$$

where a, b, c, and d are functions of ϕ and are to be determined from the known boundary conditions on the problem and the two equations previously derived. The boundary conditions on the velocity profile are:

1. No slip at the cylinder surface.
2. The definition of U_δ.
3. Continuity of shear stress at the edge of the film.
4. The differential form of the ϕ-momentum equation evaluated at the surface of the cylinder.

Mathematically, the above boundary conditions are:

1. At $\eta=0$ $\quad U_\phi=0$
2. At $\eta=1$ $\quad U_\phi=U_\delta$
3. At $\eta=1$ $\quad \tau_e=\mu_1\left(\frac{\partial U_\phi}{\partial r}\right)_{r=R+\delta} = \frac{\mu_1}{\delta}\left(\frac{\partial U_\phi}{\partial \eta}\right)_{\eta=1}$
4. At $\eta=0$ $\quad 0 = -\frac{1}{R}\frac{dp}{d\phi} + \mu_1\left[\frac{\partial}{\partial r}\left(\frac{1}{r}\frac{\partial}{\partial r}(rU_\phi)\right) + \frac{1}{r^2}\frac{\partial^2 U_\phi}{\partial \phi^2}\right]_{\eta=0}$

which reduces to:

$$\frac{1}{\mu_1 R}\frac{dp}{d\phi} = \frac{1}{\delta^2}\frac{\partial}{\partial \eta}\left\{\frac{1}{R+\delta\eta}\left[(R+\delta\eta)\frac{\partial U_\phi}{\partial \eta} + U_\phi\delta\right]\right\}_{\eta=0}$$

If the polynomial expression for U_ϕ is substituted into the above boundary conditions, the following relationships between the coefficients a, b, c, and d are obtained:

from 1: $a = 0$

from 2: $b + c + d = 1$

from 3: $b + 2c + 3d = \dfrac{\tau_e \delta}{\mu_1 U_\delta}$

from 4:

$$\frac{\delta^2}{\mu_1 R}\frac{dp}{d\phi} = \frac{\partial}{\partial \eta}\left\{U_\delta[b + 2c\eta + 3d\eta^2] + \frac{U_\phi}{U_\delta}\frac{U_\delta \delta}{R + \delta\eta}\right\}_{\eta=0}$$

$$= 2cU_\delta + U_\delta \bar{\delta} b$$

$$\text{or,} \quad 2c + \bar{\delta} b = \frac{\delta}{\mu_1 U_\delta}\bar{\delta}\frac{dp}{d\phi} .$$

For convenience a new parameter, $\tau_1 = \mu_1 \dfrac{U_\delta}{\delta}$, is introduced. This parameter has the form of a shear stress and is the viscous shear stress that would exist in the film if the profile were linear. A simultaneous solution of the above equations yields:

$$a = 0$$

$$b = -\frac{\bar{\delta}}{4 - \bar{\delta}}\frac{1}{\tau_1}\frac{dp}{d\phi} - \frac{2}{4 - \bar{\delta}}\left(\frac{\tau_e}{\tau_1} - 3\right)$$

$$c = \frac{2\bar{\delta}}{4 - \bar{\delta}}\frac{1}{\tau_1}\frac{dp}{d\phi} + \frac{\bar{\delta}}{4 - \bar{\delta}}\left(\frac{\tau_e}{\tau_1} - 3\right)$$

$$d = -\frac{1}{4 - \bar{\delta}}\frac{\bar{\delta}}{\tau_1}\frac{dp}{d\phi} + \frac{2 - \bar{\delta}}{4 - \bar{\delta}}\left(\frac{\tau_e}{\tau_1} - 3\right) + 1$$

Now $\bar{\delta} << 1$, so that the above equations may be simplified to:

$$a = 0$$

$$b = -\frac{1}{4}\frac{\bar{\delta}}{\tau_1}\frac{dp}{d\phi} - \frac{1}{2}\frac{\tau_e}{\tau_1} + \frac{3}{2}$$

$$c = \frac{1}{2}\frac{\bar{\delta}}{\tau_1}\frac{dp}{d\phi} + \frac{\bar{\delta}}{4}\frac{\tau_e}{\tau_1} - \frac{3}{4}\bar{\delta}$$

$$d = -\frac{1}{4}\frac{\bar{\delta}}{\tau_1}\frac{dp}{d\phi} + \frac{1}{2}\frac{\tau_e}{\tau_1} - \frac{1}{2}.$$

Thus, the velocity profile in the film becomes:

$$f_v = \frac{U_\phi}{U_\delta} = \frac{1}{2}(3\eta - \eta^3) - \frac{1}{2}\frac{\tau_e}{\tau_1}(\eta - \eta^3) - \frac{1}{4}\frac{\bar{\delta}}{\tau_1}\frac{dp}{d\phi}(\eta - 2\eta^2 + \eta^3) \qquad (5)$$

where the last two terms of the coefficient "c" have been neglected.

It is interesting to note that if the pressure gradient terms and the external shear terms are discarded, the velocity profile reduces to the case where similarity exists:

$$\frac{U_\phi}{U_\delta} = \frac{1}{2}(3\eta - \eta^3) . \qquad (6)$$

The velocity profile (Equation (5)) contains both the film thickness and the velocity at the edge of the film as parameters.

These two quantities are determined from the continuity equation (Equation (1)) and the ϕ-momentum equation which neglects the film

inertia and body forces (Equation (4)). Substituting the velocity profile into these equations yields:

Continuity:

$$\frac{R\dot{m}_1}{U_\delta \delta \rho_1} \sin\phi = \int_0^1 (b\eta + c\eta^2 + d\eta^3)d\eta$$

$$= \frac{b}{2} + \frac{c}{3} + \frac{d}{4}$$

$$\frac{\dot{m}_1}{\rho_a U_\infty} \frac{\sin\phi}{\frac{U_\delta}{U_\infty}\frac{\rho_1}{\rho_a}\bar{\delta}} = -\frac{1}{48}\frac{\bar{\delta}}{\tau_1}\frac{dp}{d\phi} + \frac{(2\bar{\delta} - 3)}{24}\frac{\tau_e}{\tau_1} + \frac{5 - 2\bar{\delta}}{8}$$

which simplifies by considering $\bar{\delta} << 1$ to:

$$-\frac{1}{48}\frac{\bar{\delta}}{\tau_1}\frac{dp}{d\phi} - \frac{1}{8}\frac{\tau_e}{\tau_1} + \frac{5}{8} = \frac{1}{\frac{U_\delta}{U_\infty}}\frac{\dot{m}_r}{\rho\bar{\delta}} \sin\phi \ . \qquad (7)$$

The momentum equation (Equation (4)) may be modified by realizing that

$$\tau_o = \mu_1\left(\frac{\partial U_\phi}{\partial r}\right)_{r=R} = \frac{\mu_1 U_\delta}{\delta}\frac{\partial}{\partial\eta}\left(\frac{U_\phi}{U_\delta}\right)\Bigg]_{\eta=0} = b\tau_1 \qquad (8)$$

so that

$$\frac{3}{4}\bar{\delta}\frac{1}{\rho_a U_\infty^2}\frac{dp}{d\phi} - \frac{3}{2}\frac{\tau_e}{\rho_a U_\infty^2} + \frac{3}{2}\frac{\tau_1}{\rho_a U_\infty^2} - \dot{m}_r \sin\phi\cos\phi = 0. \qquad (8)$$

Equations (7) and (8) may be solved simultaneously to eliminate the linear shear stress term, τ_1. The resulting equation is a cubic equation in the film thickness, $\bar{\delta}$:

$$\frac{1}{\rho_a U_\infty^2}\frac{dp}{d\phi}\bar{\delta}^3 - \left[\frac{3}{2}\frac{\tau_e}{\rho_a U_\infty^2} + \frac{5}{4}\dot{m}_r \sin\phi\cos\phi\right]\bar{\delta}^2 = -6\frac{\dot{m}_r}{Re_1}\sin\phi$$

For the case of potential flow around the cylinder, the pressure gradient term is given by

$$\frac{1}{\rho_a U_\infty^2}\frac{dp}{d\phi} = -4\sin\phi\cos\phi$$

so that the final equation for the film thickness is:

$$4\sin\phi\cos\phi\,\bar{\delta}^3 + \left[\frac{3}{4}\frac{\tau_e}{\frac{1}{2}\rho_a U_\infty^2} + \frac{5}{4}\dot{m}_r \sin\phi\cos\phi\right]\bar{\delta}^2 = 6\frac{\dot{m}_r}{Re_1}\sin\phi \qquad (9)$$

Equation (9) neglects the film inertia and the body forces.

The previously neglected body force term would have appeared in Equation (9) as an additional coefficient of the cubic term. This additional part of the cubic coefficient is $(gR\bar{\rho}\sin\phi)/U_\infty^2$ and is on the same order of magnitude as that part due to the pressure gradient, $4\sin\phi\cos\phi$. The body force should therefore have about the same effect on the film

thickness as the pressure gradient and the latter's effect is shown below to be of secondary importance. The neglected film inertia term and the body force term have opposite effects on the film thickness and thus have a tendency to cancel each other out.

Note that for the case when the pressure gradient is neglected, the film thickness equation becomes much more manageable as the cubic term is removed:

$$\bar{\delta}^2 = \frac{6 \frac{\dot{m}_r}{Re_1} \sin\phi}{\frac{3}{4} \frac{\tau_e}{\frac{1}{2} \rho_a U_\infty^2} + \frac{5}{4} \dot{m}_r \sin\phi\cos\phi} \tag{10}$$

If, in addition, the external shear stress is neglected, then the interesting result is that the film thickness depends only upon the free stream Reynolds number (with the properties of liquid used instead of air) and is independent of the mass flow ratio of water to air:

$$\bar{\delta}^2 = \frac{4.8}{Re_1} \sec\phi \ . \tag{11}$$

Equations (9), (10), and (11) are compared in Figure 3 for $Re = 30{,}000$ and $\dot{m}_r = 0.028$--those conditions (low Reynolds number and low water-to-air mass flow ratio) under which the pressure gradient has its greatest effect (for the range of variables investigated experimentally). From this figure it is clear that the pressure gradient (and therefore the body force) are secondary effects, but that the shear

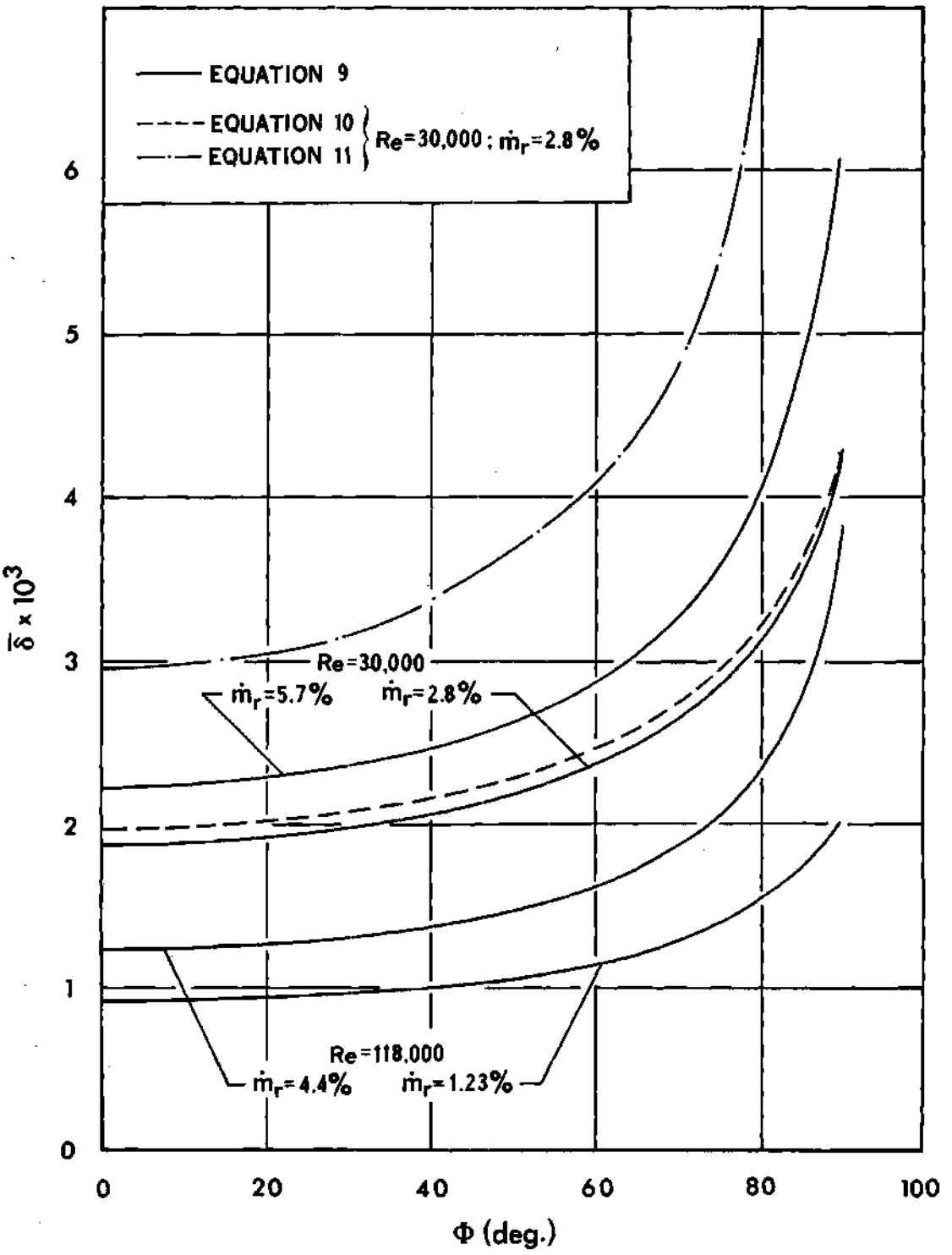

Figure 3. Analytical Film Thicknesses

stress is important. Additional evidence that the body force is not important was reported by Acrivos (2) who observed that the liquid film on his vertical cylinder travelled horizontally until separation occurred--at which point the film ran down the cylinder under the influence of gravity. Figure 3 also shows the film thickness (Equation (9)) for Re = 30,000, $\dot{m}_r = 0.057$; Re = 118,000, $\dot{m}_r = 0.0123$, and $\dot{m}_r = 0.044$.

In performing calculations involving Equations (9) and (10), some value for the external shear stress must be found. A convenient expression for the shear stress distribution around a circular cylinder is reported in reference 14 in the form of an infinite series in odd powers of the angle from the stagnation point. This so-called Blasius series expansion is the one used in all calculations in the present study.

Energy Equation

The derivation of the energy equation considers the energy fluxes associated with the control volume a-b-c-d shown in Figure 4. Under the assumption of steady flow, negligible kinetic, potential and viscous energy sources, and negligible evaporation; the energy balance may be written as

$$\int_R^{R+\delta} \rho_l c_{pl}(T - T_r)U_\phi dr\Bigg|_{\phi - \frac{\Delta\phi}{2}} + \int_R^{R+\delta} -k_l \frac{\partial T}{\partial \phi}\, dr\Bigg|_{\phi - \frac{\Delta\phi}{2}}$$

$$+ \dot{m}_l c_{pl}(T_\infty - T_r)(R + \delta)(\Delta\phi)\cos\phi - k_l\left(\frac{\partial T}{\partial r}\right)_{r=R} R(\Delta\phi)$$

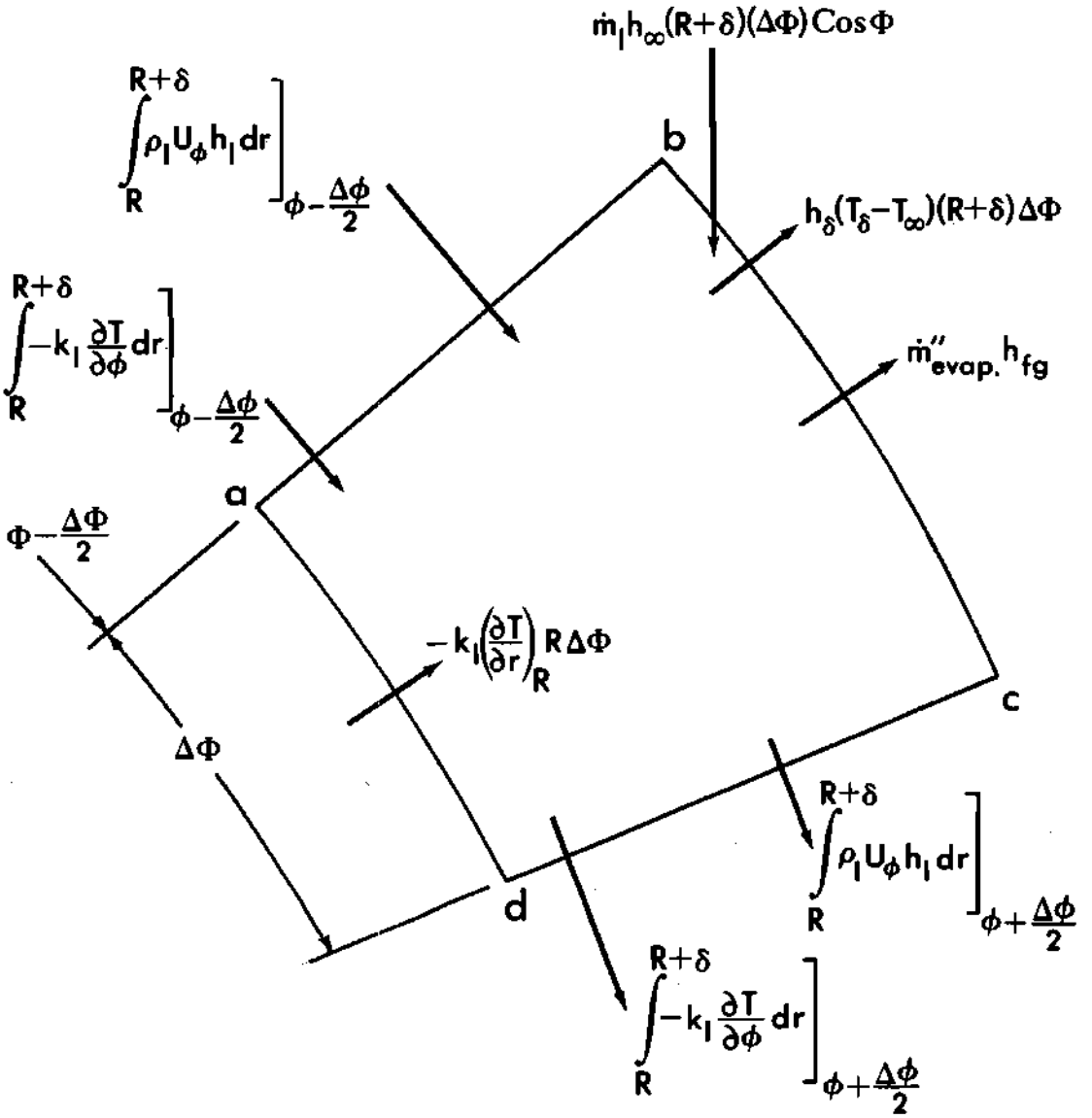

Figure 4. Control Volume abcd Showing Energy Fluxes

$$- \int_{R}^{R+\delta} \rho_l c_{pl}(T - T_r)U_\phi dr \Bigg|_{\phi + \frac{\Delta\phi}{2}} - \int_{R}^{R+\delta} -k_l \frac{\partial T}{\partial \phi} dr \Bigg|_{\phi + \frac{\Delta\phi}{2}}$$

$$- h_\delta(T_\delta - T_\infty)(R + \delta)(\Delta\phi) = 0 \qquad (12)$$

The terms in the above equation represent:

1. the enthalpy of the liquid entering face a-b
2. the heat conduction across face a-b
3. the enthalpy of the liquid drops entering face b-c
4. the heat conduction across face a-d
5. the enthalpy of the liquid leaving face c-d
6. the heat conduction across face c-d
7. the heat transfer from the film to the air through face b-c.

The reference temperature for enthalpy is designated as T_r. By expressing the values of the above functions at $\phi - \frac{\Delta\phi}{2}$ and $\phi + \frac{\Delta\phi}{2}$ in terms of their values at ϕ and their derivatives at ϕ, there results:

$$\int_{R}^{R+\delta} \rho_l c_{pl}(T - T_r)U_\phi dr \Bigg|_{\phi - \frac{\Delta\phi}{2}} = \int_{R}^{R+\delta} \rho_l c_{pl}(T - T_r)U_\phi dr -$$

$$\frac{\partial}{\partial \phi} \int_{R}^{R+\delta} \rho_l c_{pl}(T - T_r)U_\phi dr \left(\frac{\Delta\phi}{2}\right)$$

$$\int_{R}^{R+\delta} \rho_l c_{pl}(T - T_r)U_\phi dr \Bigg|_{\phi + \frac{\Delta\phi}{2}} \tilde{=} \int_{R}^{R+\delta} \rho_l c_{pl}(T - T_r)U_\phi dr +$$

$$\frac{\partial}{\partial\phi} \int_{R}^{R+\delta} \rho_l c_{pl}(T - T_r)U_\phi dr \left(\frac{\Delta\phi}{2}\right)$$

$$\int_{R}^{R+\delta} -k_l \frac{\partial T}{\partial\phi} dr \Bigg|_{\phi - \frac{\Delta\phi}{2}} \tilde{=} \int_{R}^{R+\delta} -k_l \frac{\partial T}{\partial\phi} dr \Bigg|_{\phi} - \frac{\partial}{\partial\phi} \int_{R}^{R+\delta} -k_l \frac{\partial T}{\partial\phi} dr \left(\frac{\Delta\phi}{2}\right)$$

$$\int_{R}^{R+\delta} -k_l \frac{\partial T}{\partial\phi} dr \Bigg|_{\phi + \frac{\Delta\phi}{2}} \tilde{=} \int_{R}^{R+\delta} -k_l \frac{\partial T}{\partial\phi} dr \Bigg|_{\phi} + \frac{\partial}{\partial\phi} \int_{R}^{R+\delta} -k_l \frac{\partial T}{\partial\phi} dr \left(\frac{\Delta\phi}{2}\right) .$$

Using the above results in Equation (12) and simplifying yields:

$$\rho_l c_{pl} \frac{d}{d\phi} \int_{R}^{R+\delta} (T - T_r)U_\phi dr(\Delta\phi) + k_l \frac{d}{d\phi} \int_{R}^{R+\delta} \frac{\partial T}{\partial\phi} dr(\Delta\phi) + k_l \left(\frac{\partial T}{\partial r}\right)_{r=R} R\ (\Delta\phi)$$

$$+ h_\delta(T_\delta - T_\infty)(R + \delta)(\Delta\phi) - \dot{m}_l c_{pl}(T_\infty - T_r)(R + \delta)(\cos\phi)(\Delta\phi) = 0$$

Now it is expected that conduction in the ϕ-direction will be small compared to the other effects and since the reference temperature for the liquid enthalpy is arbitrary, it is chosen to have the same value as the

free stream droplet temperature, T_∞. Under these simplifications, the energy equation becomes:

$$\rho_l c_{pl} \frac{d}{d\phi} \int_R^{R+\delta} \theta U_\phi dr = -k_l \left(\frac{\partial \theta}{\partial r}\right)_{r=R} R - h_\delta \theta_\delta R$$

where $\theta = T - T_\infty$. The energy equation may be non-dimensionalized by introducing $f_t = \frac{\theta}{\theta_o}$ and $f_v = \frac{U_\phi}{U_\delta}$ along with the co-ordinate η.

$$\frac{d}{d\phi}\left[\frac{U_\delta}{U_\infty}\bar{\delta}\int_0^1 f_t f_v d\eta\right] = -\frac{\alpha_l}{\bar{\delta} U_\infty R}\left(\frac{\partial f_t}{\partial \eta}\right)_{\eta=0} - \frac{h_\delta}{\rho_l c_{pl} U_\infty}(f_t)_{\eta=1}$$

Further simplification is obtained with the realization that:

$$\frac{h_\delta}{\rho_l c_{pl} U_\infty} = \frac{h_\delta D}{k_a}\frac{k_a}{k_l}\frac{k_l}{\mu_l c_{pl}}\frac{\mu_l}{\rho_l U_\infty D} = Nu_\delta \frac{k_a}{k_l}\frac{1}{Pr_l Re_l}$$

and

$$\frac{\alpha_l}{U_\infty R} = \frac{2\,k_l}{\rho_l c_{pl} U_\infty D} = 2\frac{k_l}{\mu_l c_{pl}}\frac{\mu_l}{\rho_l U_\infty D} = \frac{2}{Pr_l Re_l}$$

so that the final form of the energy equation is:

$$\frac{d}{d\phi}\left[\frac{U_\delta}{U_\infty}\bar{\delta}\int_0^1 f_t f_v d\eta\right] = -\frac{2}{Pr_l Re_l}\left[\frac{1}{\bar{\delta}}\left(\frac{\partial f_t}{\partial \eta}\right)_{\eta=0} + \frac{k_a}{k_l}\frac{Nu_\delta}{2}(f_t)_{\eta=1}\right] \qquad (13)$$

The above equation neglects the influence of conduction in the ϕ-direction (see Appendix C), kinetic and potential energy changes, viscous dissipation, and evaporation (see Appendix B).

Solution of the Energy Equation

The energy equation may be solved for the temperature distribution in the film if a form for this distribution is assumed. As in the case of the velocity profiles, a polynomial distribution is assumed:

$$\theta(\eta,\phi) = \theta_\delta(\phi) f(\eta,\phi)$$

where

$$f(\eta,\phi) = a_t(\phi) + b_t(\phi)\eta + c_t(\phi)\eta^2 + d_t(\phi)\eta^3$$

and a_t, b_t, c_t, and d_t are functions of ϕ and are to be determined from the known boundary conditions on the temperature profile. These boundary conditions are:

1. at $\eta=0$ $\quad \theta = \theta_o$

2. at $\eta=1$ $\quad \theta = \theta_\delta$

3. at $\eta=0$ $\quad \frac{\partial}{\partial r}\left[r \frac{\partial \bar{T}}{\partial r}\right] = 0 \quad \therefore \quad \bar{\delta}\left(\frac{\partial f}{\partial \eta}\right)_{\eta=0} + \left(\frac{\partial^2 f}{\partial \eta^2}\right)_{\eta=0} = 0$

4. at $\eta=1$ $\quad -k_1\left(\frac{\partial T}{\partial r}\right)_{r=R+\delta} = h_\delta(T_\delta - T_\infty)$

$$\therefore \left(\frac{\partial \bar{f}}{\partial \eta}\right)_{\eta=1} = -\frac{k_a}{k_1}\frac{\bar{\delta}}{2} Nu_\delta$$

The third boundary condition results from the differential form of the

energy equation evaluated at the surface of the cylinder. If the assumed form for the temperature profile is substituted into the boundary conditions, then the following four equations result:

1. $a_t = \frac{\theta_o}{\theta_\delta}$

2. $a_t + b_t + c_t + d_t = 1$

3. $\bar{\delta} b_t + 2c_t = 0$

4. $b_t + 2c_t + 3d_t = -\frac{k_a}{k_1}\frac{Nu_\delta}{2}\bar{\delta}$.

Note that the third equation above says that c_t is of order $\bar{\delta}$ when compared with b_t. This means that the terms involving c_t may be neglected in the analysis because c_t only occurs in those equations which also involve b_t. A simultaneous solution of the above equations yields the following expressions for the coefficients of the temperature profile:

1. $a_t = \frac{\theta_o}{\theta_\delta}$

2. $b_t = \frac{3}{2}\left(1 - \frac{\theta_o}{\theta_\delta}\right) + \frac{k_a}{k_1}\frac{Nu_\delta}{4}\bar{\delta}$

3. c_t = negligible

4. $d_t = -\frac{1}{2}\left(1 - \frac{\theta_o}{\theta_\delta}\right) - \frac{k_a}{k_1}\frac{Nu_\delta}{4}\bar{\delta}$

When these values are substituted into the temperature profile, the resulting expression for f is:

$$f = \frac{\theta}{\theta_\delta} = \frac{\theta_o}{\theta_\delta} + \left[\frac{3}{2}\left(1 - \frac{\theta_o}{\theta_\delta}\right) + \frac{k_a}{k_1}\frac{Nu_\delta}{4}\bar{\delta}\right]\eta - \left[\frac{1}{2}\left(1 - \frac{\theta_o}{\theta_\delta}\right) + \frac{k_a}{k_1}\frac{Nu_\delta}{4}\bar{\delta}\right]\eta^3 .$$

The energy equation, however, requires f_t which is easily obtained by multiplying f by $\frac{\theta_\delta}{\theta_o}$. After some manipulation f_t is expressed as:

$$f_t = 1 - \frac{3}{2}\left(1 - \frac{\theta_\delta}{\theta_o}\right)\eta + \frac{1}{2}\left(1 - \frac{\theta_\delta}{\theta_o}\right)\eta^3 + \frac{\theta_\delta}{\theta_o}\frac{k_a}{k_1}\frac{Nu_\delta}{4}\bar{\delta}(\eta - \eta^3) \qquad (14)$$

A further simplification of the temperature profile results with an estimation of the magnitude of the various terms. Taking the values for k_a and k_1 from reference (15) at a temperature of 100 °F, the ratio of k_a to k_1 is found to be approximately 0.04. It is felt that the Nusselt number for the flow of air over the film will be on the same order as the Nusselt number that would exist if the air were flowing over a dry cylinder. For the Reynolds numbers involved in this study this Nusselt number is on the order of 500 or less. The temperature ratio, $\frac{\theta_\delta}{\theta_o}$, will always be less than unity and therefore the last term in the temperature profile is of order $\bar{\delta}$ when compared with the other terms (which are of order unity). The last term is therefore negligible compared to the other terms. The resulting temperature profile is:

$$f_t = 1 - \frac{3}{2}\left(1 - \frac{\theta_\delta}{\theta_o}\right)\eta + \frac{1}{2}\left(1 - \frac{\theta_\delta}{\theta_o}\right)\eta^3 \qquad (15)$$

The same arguments can be used in considering the energy Equation (13). In this equation f_t evaluated at the edge of the film is of order unity or less, while an order of magnitude analysis on $\left(\frac{\partial f_t}{\partial \eta}\right)_{\eta=0}$ indicates that this term is of order unity also because both the dependent and independent variables are of order unity. Thus, the last term in Equation

(13) is negligible compared to the other terms and may be ignored. The energy equation is therefore:

$$\frac{d}{d\phi}\left[\frac{U_\delta}{U_\infty}\bar{\delta}\int_0^1 f_t f_v d\eta\right] = -\frac{2}{Pr_1 Re_1}\frac{1}{\bar{\delta}}\left(\frac{\partial f_t}{\partial \eta}\right)_{\eta=0} \qquad (16)$$

The effect of the above order analysis is to ignore the influence of heat losses from the edge of the film both on the energy equation and the temperature profile. Later it will be possible to see that this simplification is justified in view of the large heat transfers observed experimentally when water droplets are added to the air stream before it intercepts the cylinder.

Before proceeding directly with the solution of the energy equation, it is necessary to reconsider the hydrodynamic part of the problem because the velocity profile is an essential part of the energy equation. The expression for f_v which contains the shear stress and the pressure gradient terms is rather unwieldy and, when substituted into the energy equation, results in a very complicated equation which is very tedious to solve. Fortunately, the analytical results for f_v are very closely represented by the simple expression: $f_v = \frac{1}{4}(5\eta - \eta^3)$. A comparison of the various expressions for f_v can be found in Figure 5. It is interesting to note that this simple expression for f_v is really the average between f_v as given by Equation (6) and $f_v = \eta$, which is a linear profile. If this profile is used then the energy equation becomes more amenable to solution. The integral $\int_0^1 f_v f_t d\eta$ can be evaluated as:

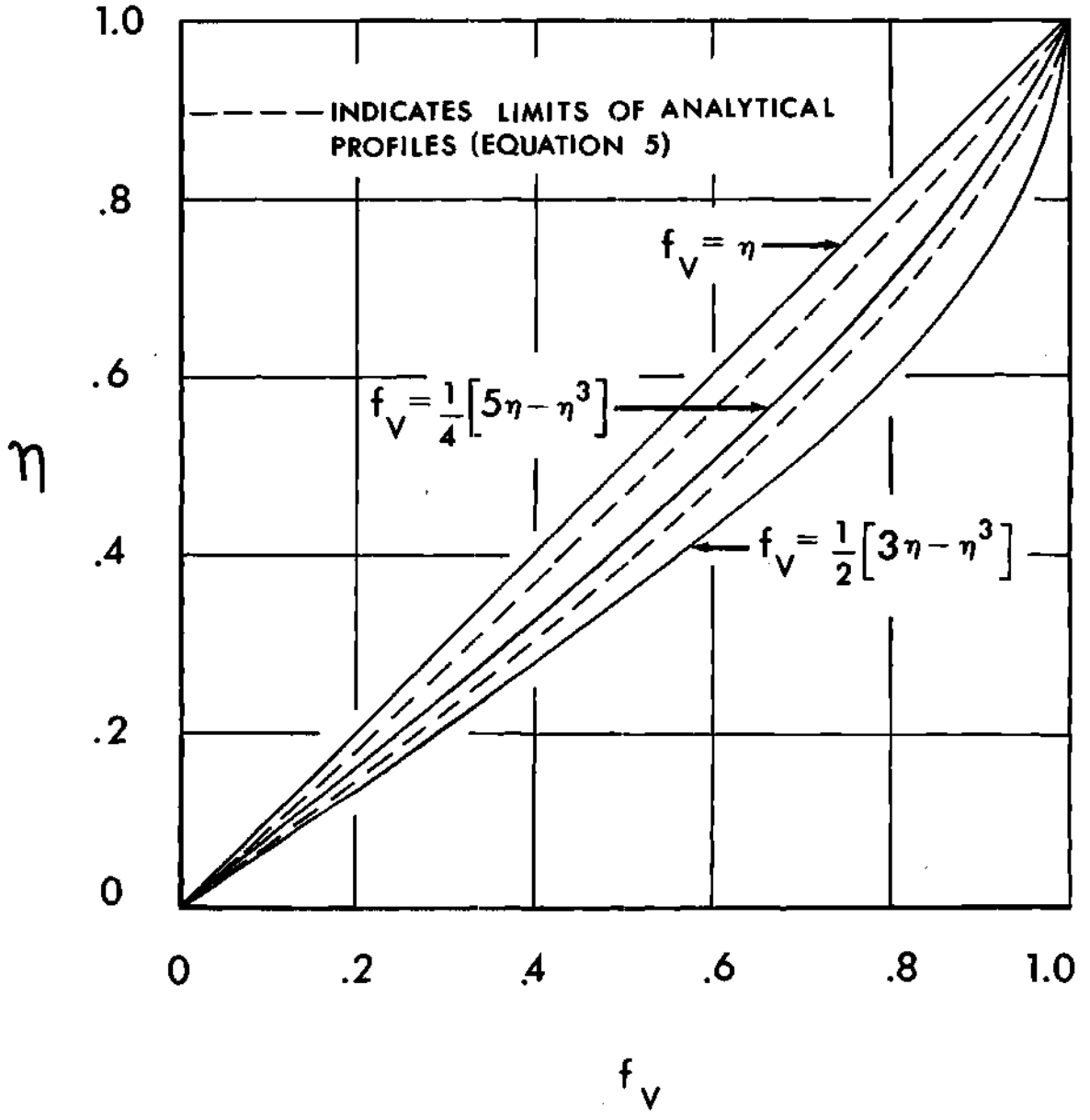

Figure 5. Analytical Velocity Profiles in the Film

$$\int_0^1 f_v f_t d\eta = \int_0^1 \frac{1}{4}\left[5\eta - \eta^3\right]\left[1 - \frac{1}{2}\left(1 - \frac{\theta_\delta}{\theta_o}\right)\left(3\eta - \eta^3\right)\right]d\eta$$

$$= \frac{9}{16} - \frac{31}{70}\left(1 - \frac{\theta_\delta}{\theta_o}\right)$$

and $$\left.\frac{\partial f_t}{\partial \eta}\right|_{\eta=0} = -\frac{3}{2}\left(1 - \frac{\theta_\delta}{\theta_o}\right) .$$

The energy Equation (16) thus becomes

$$\frac{d}{d\phi}\left\{\frac{U_\delta}{U_\infty}\bar{\delta}\left[\frac{9}{16} - \frac{31}{70}\left(1 - \frac{\theta_\delta}{\theta}\right)\right]\right\} = \frac{3}{Pr_1 Re_1}\frac{1}{\bar{\delta}}\left(1 - \frac{\theta_\delta}{\theta_o}\right)$$

which, upon carrying out the differentiation and simplifying, becomes:

$$\left(1 - \frac{\theta_\delta}{\theta}\right)\left[-\frac{31}{70}\frac{d}{d\phi}\left(\frac{U_\delta}{U_\infty}\bar{\delta}\right) - \frac{3}{Pr_1 Re_1}\frac{1}{\bar{\delta}}\right] + \frac{9}{16}\frac{d}{d\phi}\left(\frac{U_\delta}{U_\infty}\bar{\delta}\right) =$$

$$\frac{31}{70}\left(\frac{U_\delta}{U_\infty}\bar{\delta}\right)\frac{d}{d\phi}\left(1 - \frac{\theta_\delta}{\theta_o}\right) \qquad (17)$$

which is a first order, linear, ordinary differential equation.

Equation (17) may be written in a more recognizable form as

$$\frac{dy}{d\phi} + P(\phi)y = Q(\phi) \qquad \text{where } y = 1 - \frac{\theta_\delta}{\theta_o} ,$$

$$P(\phi) = \frac{d}{d\phi}\left[\ln\left(\frac{U_\delta}{U_\infty}\bar{\delta}\right)\right] + \frac{210}{31}\frac{1}{Pr_1 Re_1}\frac{U_\infty}{U_\delta}\frac{1}{\bar{\delta}^2},$$

and

$$Q(\phi) = \frac{315}{248}\frac{U_\infty}{U_\delta}\frac{1}{\bar{\delta}}\frac{d}{d\phi}\left(\frac{U_\delta}{U_\infty}\bar{\delta}\right).$$

The solution to this equation is found with the aid of an integrating factor (16):

$$ye^{\int P d\phi} = \int Qe^{\int P d\phi}\, d\phi + C$$

where C is the constant of integration. Because the expressions for P and Q are not simple, the integrations indicated in the solution are not readily found except by numerical means.

It is felt that the term in the energy equation which involves the temperature gradient around the cylinder represents a secondary effect and can be neglected. A justification of this may be found in Appendix C. If this term is discarded, the energy equation is no longer a differential equation and as a result the interface temperature, θ_δ, is easily obtained:

$$1 - \frac{\theta_\delta}{\theta_o} = \frac{\frac{9}{16}\frac{d}{d\phi}\left(\frac{U_\delta}{U_\infty}\bar{\delta}\right)}{\frac{31}{70}\frac{d}{d\phi}\left(\frac{U_\delta}{U_\infty}\bar{\delta}\right) + \frac{3}{Re_1 Pr_1}\frac{1}{\bar{\delta}}} \qquad (18)$$

Once $1 - \frac{\theta_\delta}{\theta_o}$ is known, the local heat transfer coefficient, h_L, may be found from its definition as:

$$h_L(T_o - T_\infty) = -k_1 \left(\frac{\partial T}{\partial r}\right)_{r=R}$$

After rearranging and introducing the non-dimensional variables the above equation becomes:

$$Nu_L \equiv \frac{h_L D}{k_1} = \frac{3}{\bar{\delta}} \left(1 - \frac{\theta_\delta}{\theta_o}\right) \tag{19}$$

In order to get numerical values for the Nusselt number it is necessary to evaluate $\frac{d}{d\phi}\left(\frac{U_\delta}{U_\infty}\bar{\delta}\right)$. By using Equation (8) without the pressure gradient term:

$$\tau_1 \equiv \frac{\mu_1 U_\delta}{R\bar{\delta}} = \tau_e + \frac{2}{3}\dot{m}_r \rho_a U_\infty^2 \sin\phi\cos\phi$$

which may be rearranged to give:

$$\frac{U_\delta}{U_\infty}\bar{\delta} = \frac{1}{2}\frac{\mu_a}{\mu_1} Re\bar{\delta}^2 \left[\frac{\frac{1}{2}\frac{\tau_e}{\rho_a U_\infty^2}}{} + \frac{2}{3}\dot{m}_r \sin\phi\cos\phi\right]$$

For no pressure gradient, Equation (10) may be used to express $\bar{\delta}^2$. The resultant equation for $\frac{U_\delta}{U_\infty}\bar{\delta}$ is (after much rearranging):

$$\frac{U_\delta}{U_\infty}\bar{\delta} = 12\frac{\dot{m}_r}{\bar{\rho}}\sin\phi\left[\frac{\bar{T}AU + \frac{2}{3}\dot{m}_r\sqrt{2Re}\,\sin\phi\cos\phi}{6\ TAU + 5\dot{m}_r\sqrt{2Re}\,\sin\phi\cos\phi}\right]$$

where

$$TAU \equiv \frac{\tau_e \sqrt{\frac{R_e}{2}}}{\frac{1}{2}\rho_a U_\infty^2} = 6.973\phi - 2.732\phi^3 + \cdots$$

and is the Blasius series as mentioned in the discussion of the solution of the hydrodynamic problem.

Differentiating the above expression to find the required derivative yields

$$\frac{d}{d\phi}\left[\frac{U_\delta}{U_\infty}\bar{\delta}\right] = 12\,\frac{\dot{m}_r}{\bar{\rho}}\left\{\cos\phi\left[\frac{TAU + \frac{2}{3}\dot{m}_r\sqrt{2R_e}\,\sin\phi\cos\phi}{6\,TAU + 5\dot{m}_r\sqrt{2R_e}\,\sin\phi\cos\phi}\right] + \right.$$

$$\left. \dot{m}_r\sqrt{2R_e}\,\sin\phi\left[\frac{TAU'\sin\phi\cos\phi - TAU(1 - 2\sin^2\phi)}{(6TAU + 5\dot{m}_r\sqrt{2R_e}\,\sin\phi\cos\phi)^2}\right]\right\}$$

where

$$TAU' = \frac{d}{d\phi}(TAU) = 6.973 - 8.196\phi + \cdots \qquad (20)$$

The procedure for obtaining the local Nusselt number is:

1. Choose the desired values for $\dot{m}_r$ and Re and calculate $\frac{d}{d\phi}\left(\frac{U_\delta}{U_\infty}\bar{\delta}\right)$ using Equation (20),

2. Calculate $\bar{\delta}$ by using either Equation (9) or (10),

3. Substitute the above values into Equation (18) and solve for $1 - \frac{\theta_\delta}{\theta_o}$,

4. Utilize the above results for $1 - \frac{\theta_\delta}{\theta_o}$ and $\bar{\delta}$ to calculate Nu_L from Equation (19).

A digital computer was used to calculate the effects of ignoring the temperature derivative in Equation (17) (see Appendix C). All the analytical results were programmed on a Burroughs B-5500 digital computer so that an input of $\dot{m}_r$ and Re resulted in an output of h_L, $\bar{\delta}$, U_δ, θ_δ, and U_ϕ as a function of η. This information was generated for angles of 1° to 90° in 1° increments. It is interesting to note that although both Re_l and Pr_l are both very temperature dependent, their product (which is called the Peclet number, Pe_l) is not. The solution to the energy equation, therefore, is insensitive to the temperature at which the fluid properties are evaluated and the local Nusselt number is only a function of the free stream Reynolds number, Re, and the water-to-air mass flow ratio, $\dot{m}_r$.

CHAPTER III

EQUIPMENT AND INSTRUMENTATION

Equipment

The equipment involved in the experimental portion of this investigation consisted of a closed loop wind tunnel, a spray nozzle and its associated equipment, a heated test cylinder, and recorders to monitor all significant temperatures. Detailed specifications of all equipment and instruments are given in Appendix E.

Wind Tunnel

The wind tunnel is shown in Figures 6 and 7. A closed loop design was chosen for two reasons:

1. A closed loop design permits the air in the tunnel to become saturated. It is then possible to introduce the spray water at the same temperature as the air and, since the air is saturated, no droplet evaporation occurs. If the air is not saturated, some evaporation of the droplets occurs and there results some uncertainty about the air and droplet temperatures as they intercept the cylinder. The problem of measuring the droplet temperature becomes a very formidable one because the instrument used is subjected to evaporative cooling when it is inserted into the air stream. Smith (7), who did not use a closed loop design, introduced his spray at the air wet bulb temperature in anticipation that the droplet temperature would not change. He admitted the shortcomings of his tunnel, however, when he wrote, "Ideally, it is

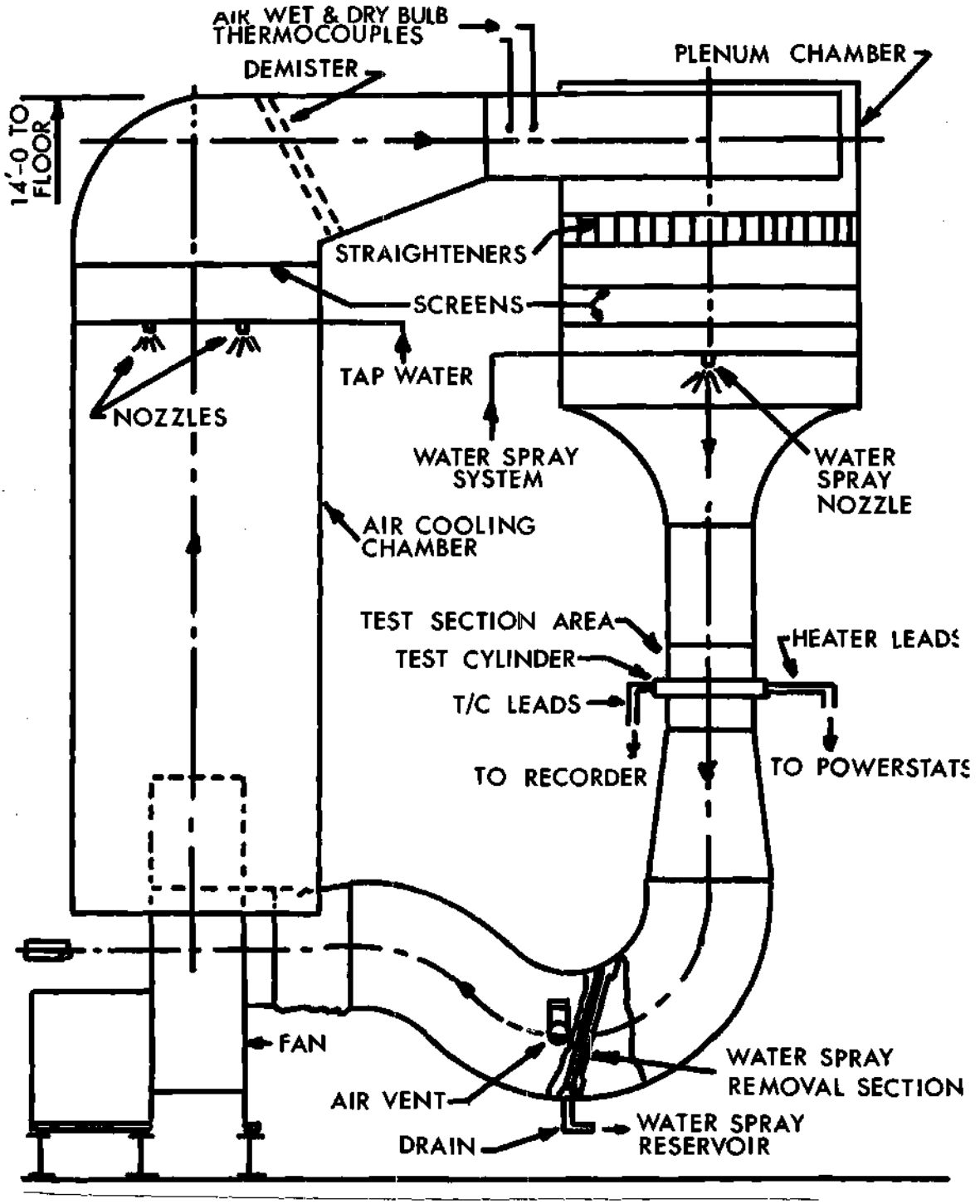

Figure 6. Schematic of the Wind Tunnel (Saterbak, Ref. 9)

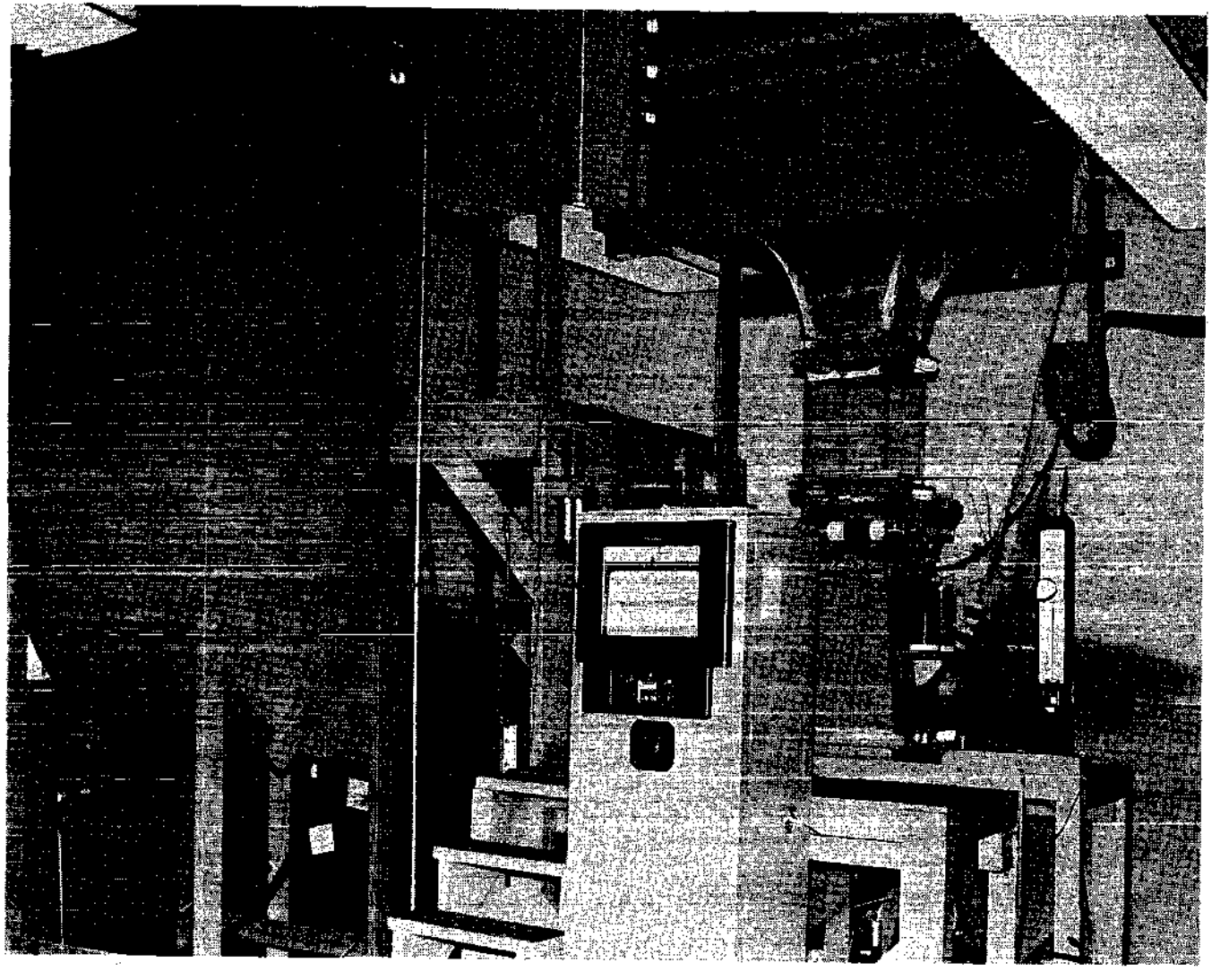

Figure 7. Photograph of the Wind Tunnel

desirable to operate under isothermal conditions, in which case, the incoming air will be water saturated and at the same temperature as the inlet water."

2. It was also felt that better control could be maintained over the air temperature with a closed loop design. An open loop is subjected to fluctuations in the air supply temperature which may become significant during a test which lasts for several hours.

It was felt that these advantages justified the additional equipment required to cool the air as it circulated through the system. The closed loop resulted in a rather high turbulence level (6 per cent) when compared with that which would exist for an open loop design, but this disadvantage was felt to be a fair price for the added control inherent in the closed loop design.

The tunnel was constructed from 1/4-inch and 1/2-inch thick grade "AA" marine plywood and was finished on the inside with several coats of polyurethane varnish. The various sections of the tunnel were made separately and were bolted together using gaskets and aluminum angle flanges. Although there were some minor leaks, the system performed extremely well and shows no signs of deterioration after a year of almost daily use. The maximum velocity measured in the test section was approximately 160 feet per second.

Air entered the large (approximately 4x4x4 feet) plenum chamber where it passed through a set of flow straighteners followed by two 16x18 mesh screens. After passing through the screens the air entered the aluminum converging nozzle which discharged into the lead-in section. This plexiglass lead-in section had a 12-inch square cross-section and

was 18 inches long. Because the tunnel was also used for studies involving a wedge (8), the test section was removable and consisted of a 12-inch square plexiglass section 12 inches long. After leaving the test section the air and the entrained water droplets passed through a diffuser which lowered the velocity by increasing the flow area from 1 ft^2 to 2 $\frac{1}{4}$ ft^2. In order to prevent excessive carryover of the spray water into the fan, a separator section was provided. This curved section caused the entrained droplets to move to the outside wall where they were removed along with the rest of the water which streamed down the walls of the tunnel. This water was directed back to the spray sump tank.

The air then entered the 6,000 c.f.m. capacity fan, passed through an adjustable damper, and entered the cooling chamber which was equipped with shower heads supplied with city water. By being exposed to the cool (70°F) city water, the air was both cooled and saturated so that the relative humidity of the air entering the plenum was always close to 100 per cent. A screen was located in the upper portion of the cooling chamber to assist in damping out turbulence and to prevent large slugs of water from being carried out of the chamber. A demister filter was placed in the duct leading from the cooling chamber to the plenum. This duct also contained the thermocouples for recording the wet and dry bulb temperatures of the air. Detailed drawings of the wind tunnel are presented in reference 8.

Spray System

The water spray was generated by pumping water through a Delavan SQ-10 spray nozzle. This nozzle was designed to produce a square,

uniformly distributed spray pattern and the manufacturer is equipped to determine the droplet size distribution to be expected from this nozzle (17). The distribution for the SQ-10 nozzle is shown in Figure 8. Water for the pump was supplied from an aluminum sump fitted with a float valve which allowed make-up water (from the city lines) to enter as required. The sump also had a drain which was opened slightly to keep cool make-up water entering the tank as an aid in maintaining a given spray water supply temperature. Two 500-watt heaters were also used, when necessary, to heat the spray water in the sump.

Water from the sump entered a turbine pump which raised the pressure to about 250 p.s.i.g. The water then passed through an aircraft type hydraulic system filter, a pressure regulator, and up to the nozzle which was located just below the second screen in the plenum. Two thermocouples were inserted into wells in the nozzle supply line--one was connected to the main recorder, while the other was used as the input to an automatic recorder-controller unit which adjusted the voltage to the sump heaters in order to maintain the spray temperature to within ±1°F of the air temperature. A schematic diagram of the spray system is shown in Figure 9.

Test Cylinder

In order to evaluate the local heat transfer coefficients around a cylinder, the definition of this coefficient

$$h_L = \frac{\dot{Q}_L}{A(T_c - T_\infty)}$$

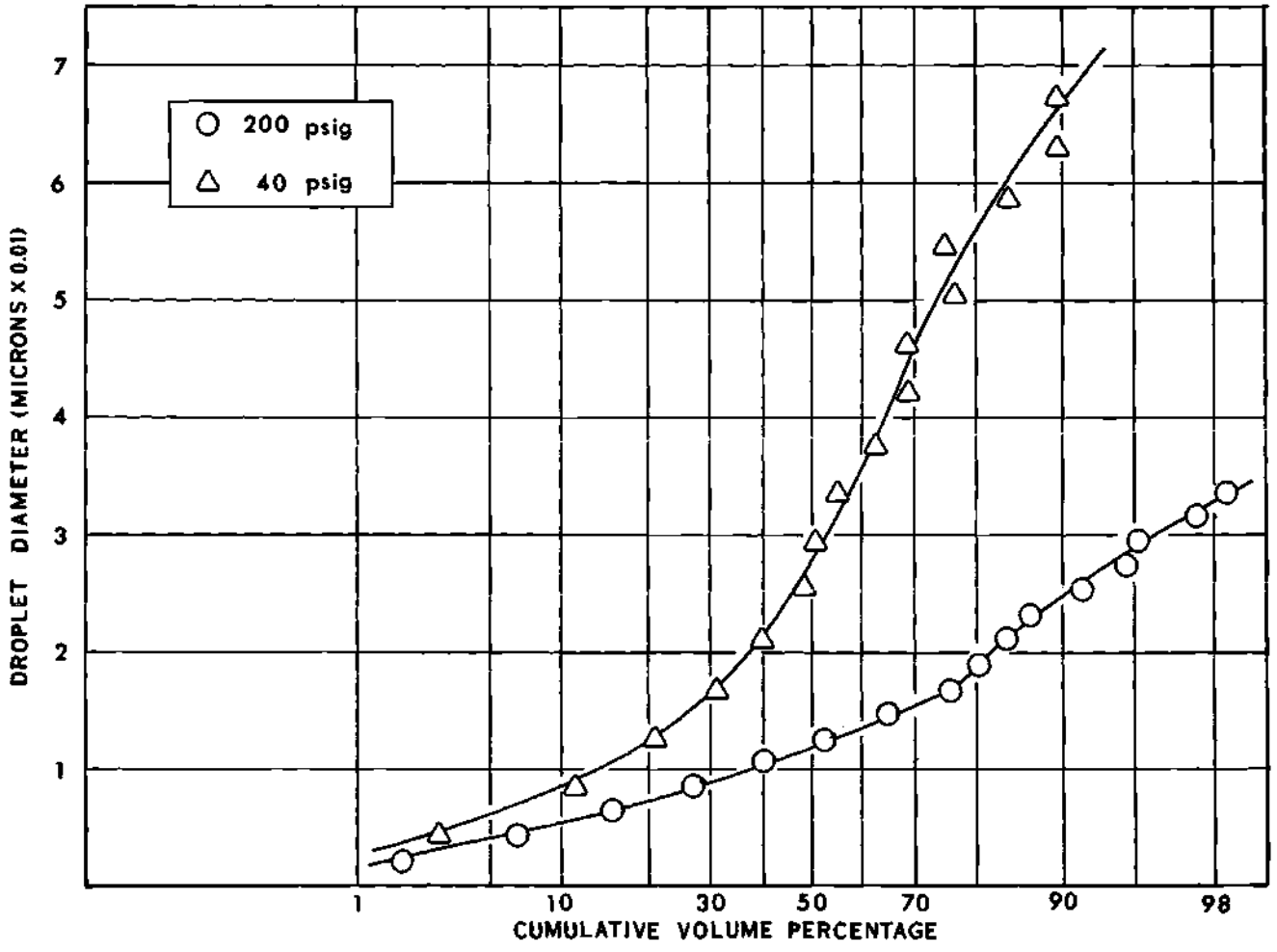

Figure 8. Droplet Size Distributions from the SQ-10 Nozzle

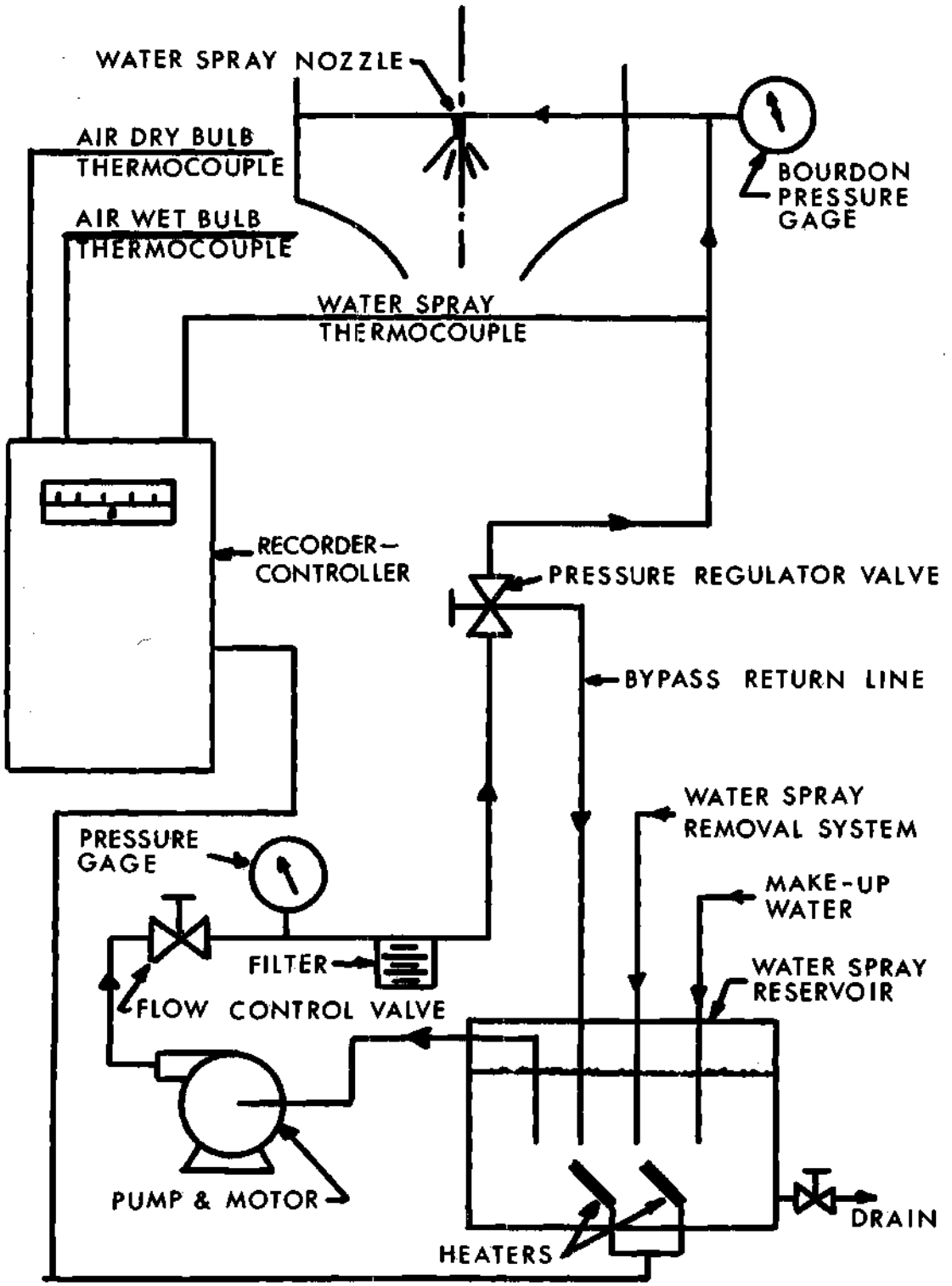

Figure 9. Schematic of the Spray System (Saterbak, Ref. 9)

requires that the local heat flux, $\dot{Q}_L$, the area, A, and the temperature difference, $T_o - T_\infty$, be known. The analytical development indicates that the value used for T_∞ should be the droplet temperature.

A test cylinder was designed and constructed so that the above quantities could be determined for each of 12 30-degree segments around a cylinder. This test cylinder is shown in Figure 10 and consisted of a 4-inch long, 3-inch diameter brass rod machined in such a manner that it was divided into 12 segments. Each segment was thermally insulated from its neighbors by two slots filled with a silica aerogel having a thermal conductivity of about 0.014 Btu/hr-ft-°F (18). The interior of the test section was also filled with this material to guard against internal heat transfer between segments via the inside cavity. Each segment was fitted with an electric cartridge heater of either 500, 250, or 125 watts, depending upon the location of the segment. The heaters were soldered into place.

Teflon-coated copper constantan thermocouples (30-gauge) were used to determine the surface temperature of the cylinder. Each thermocouple (one for each segment) was positioned in a slot (see Figure 10) which ran from the center of the segment to the end of the brass section. After each slot was tinned with solder, a thermocouple was laid in the slot with its junction protruding up slightly, and solder was then melted around the thermocouple wires to hold them in place. After the solder hardened, the surface of the cylinder was filed, sanded, and polished smooth so that there were no surface irregularities (except in color) due to the presence of the thermocouples. In this position the thermocouple lead wires ran along an isotherm for two inches from the measuring

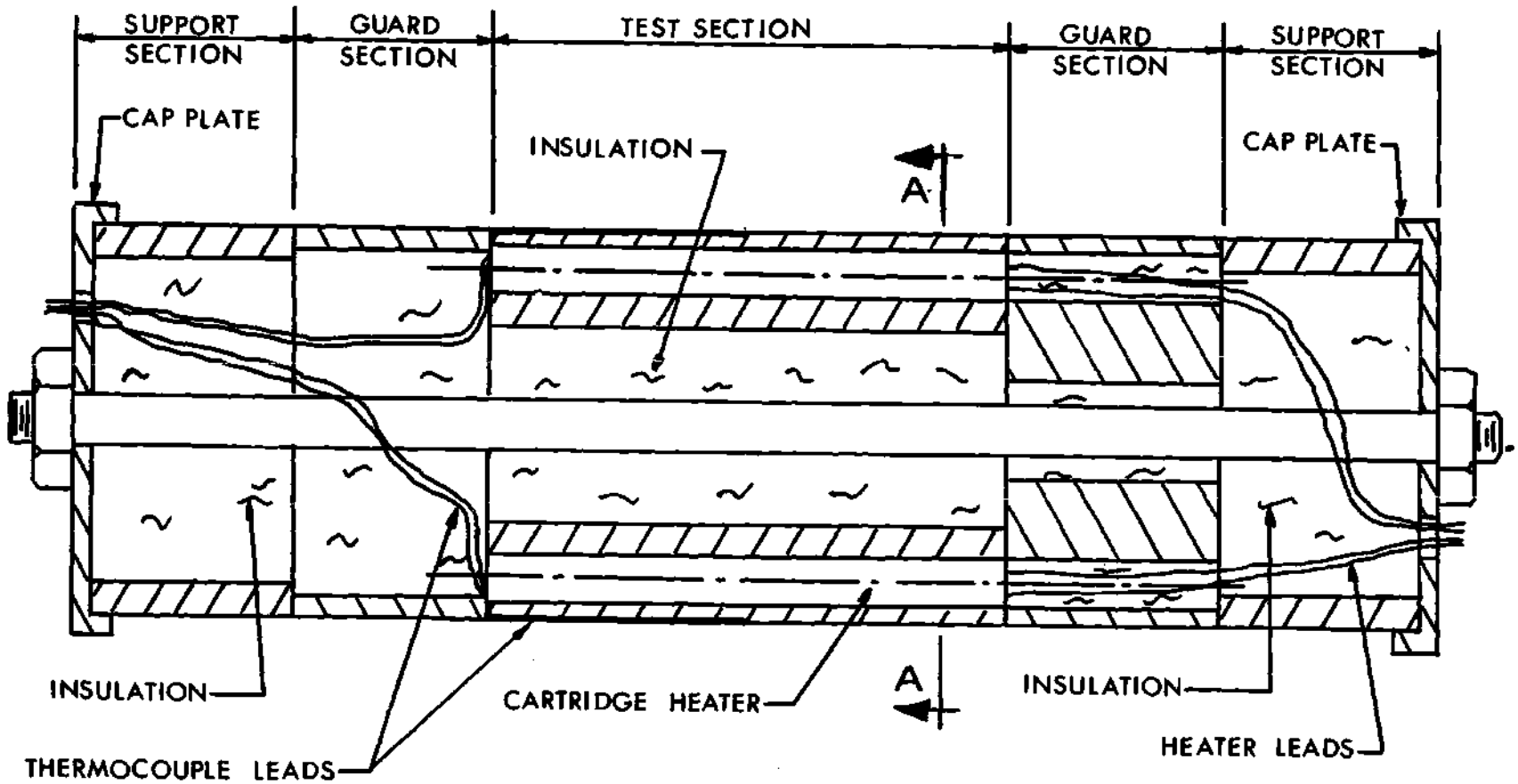

SIDE VIEW

Figure 10. Test Cylinder

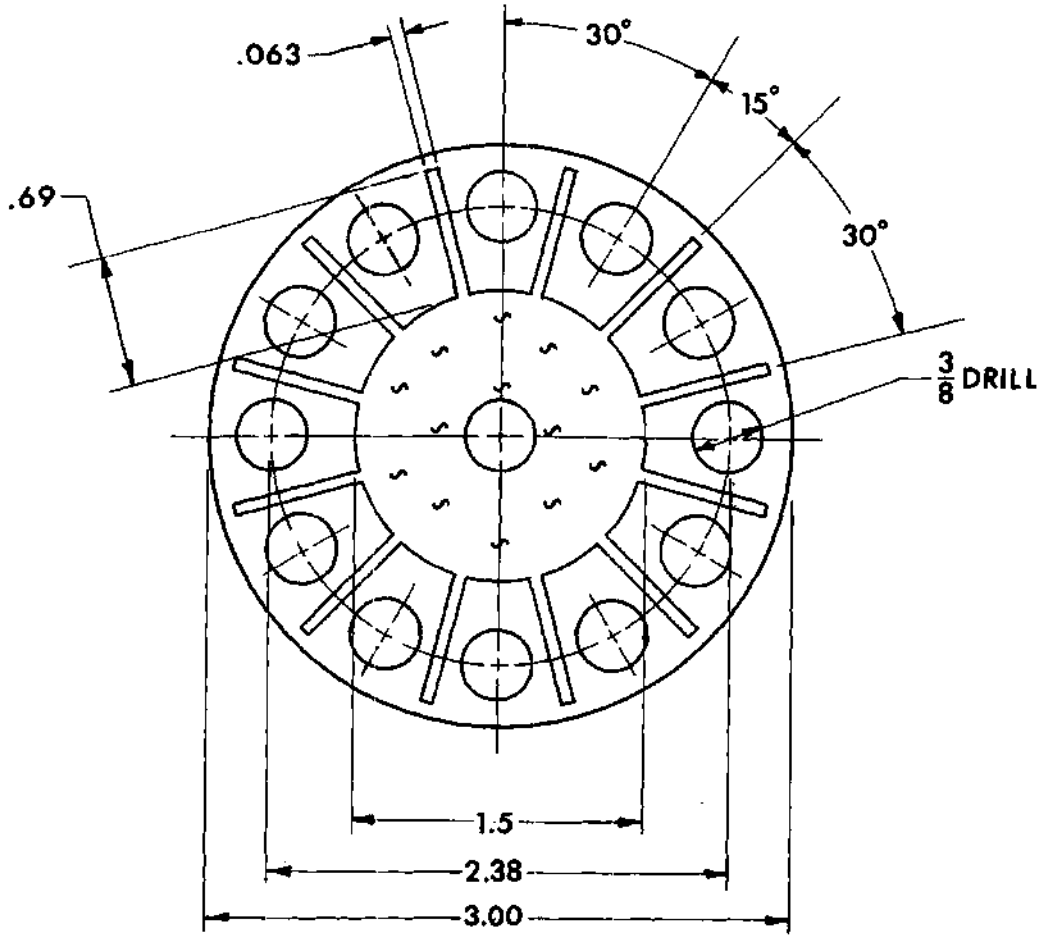

SECTION A-A

Figure 10. Test Cylinder (Continued)

junction--thus minimizing any errors in temperature measurement due to heat conduction from the junction. Since a teflon guard section was used, the slot ran down the end of the brass section to prevent the thermocouple wires from being crushed between the brass and the teflon. Before further assembly was attempted, the thermocouples were calibrated by immersing the entire brass section in a constant temperature bath. The calibration procedure is discussed further in the section labelled "Procedure."

To prevent any significant end conduction, the brass test section was supported in place on each end by a teflon guard section filled with insulation. The entire test piece was completed by the addition of two aluminum end pieces which ran through and were supported by the tunnel walls. The assembly was held together by a through-bolt bearing against the brass end caps (see Figure 10). Each joint was coated with a silicon rubber sealer before the through-bolt was tightened.

Although the brass was polished, it soon became obvious that the polished surface would not support a continuous film and consequently an oxide was allowed to form on the brass surface. This dull oxide permitted a continuous liquid film to be formed.

Auxiliary Equipment

Auxiliary equipment used included a recorder-controller which was mentioned earlier in conjunction with the spray system, a 16-channel multi-point recorder which monitored the cylinder thermocouples and the air temperatures, and 12 powerstats which supplied regulated and variable voltages for the heaters.

Instrumentation

The instrumentation used in the study involved those instruments necessary to measure cylinder and air temperatures, power input to the heaters, air velocity and the mass flow rate of droplets.

Cylinder Temperature

As reported earlier, copper-constantan thermocouples were mounted in the surface of the cylinder. Each wire of every thermocouple ran to an ice bath (separate baths were used for the + copper leads and the - constantan leads) where the reference junction was maintained at 32°F by crushed ice and water. Copper lead wires were run from the ice baths to a multi-point recorder which was set to indicate and record each temperature approximately once every 30 seconds. The recorder was wired in such a manner that the output from any thermocouple could be read directly by means of a millivolt potentiometer.

Air Temperature

In attempting to report temperatures in two-component flow one is faced with the difficulty of determining what temperature an instrument is indicating when it is placed in a two-component stream. Dussourd (19) recommended separating the air and droplets before measuring the temperature of either component. The device he used resembles closely the apparatus employed in this study to measure the droplet flow rate (see Figure 13). In the present study separation of the droplets from the air was accomplished by the device shown in Figure 11. Air and droplets enter the device through the inlet which faces directly into the stream of air and water. The entrained droplets and most of the air continue through the device and leave at the bottom exit opening. This

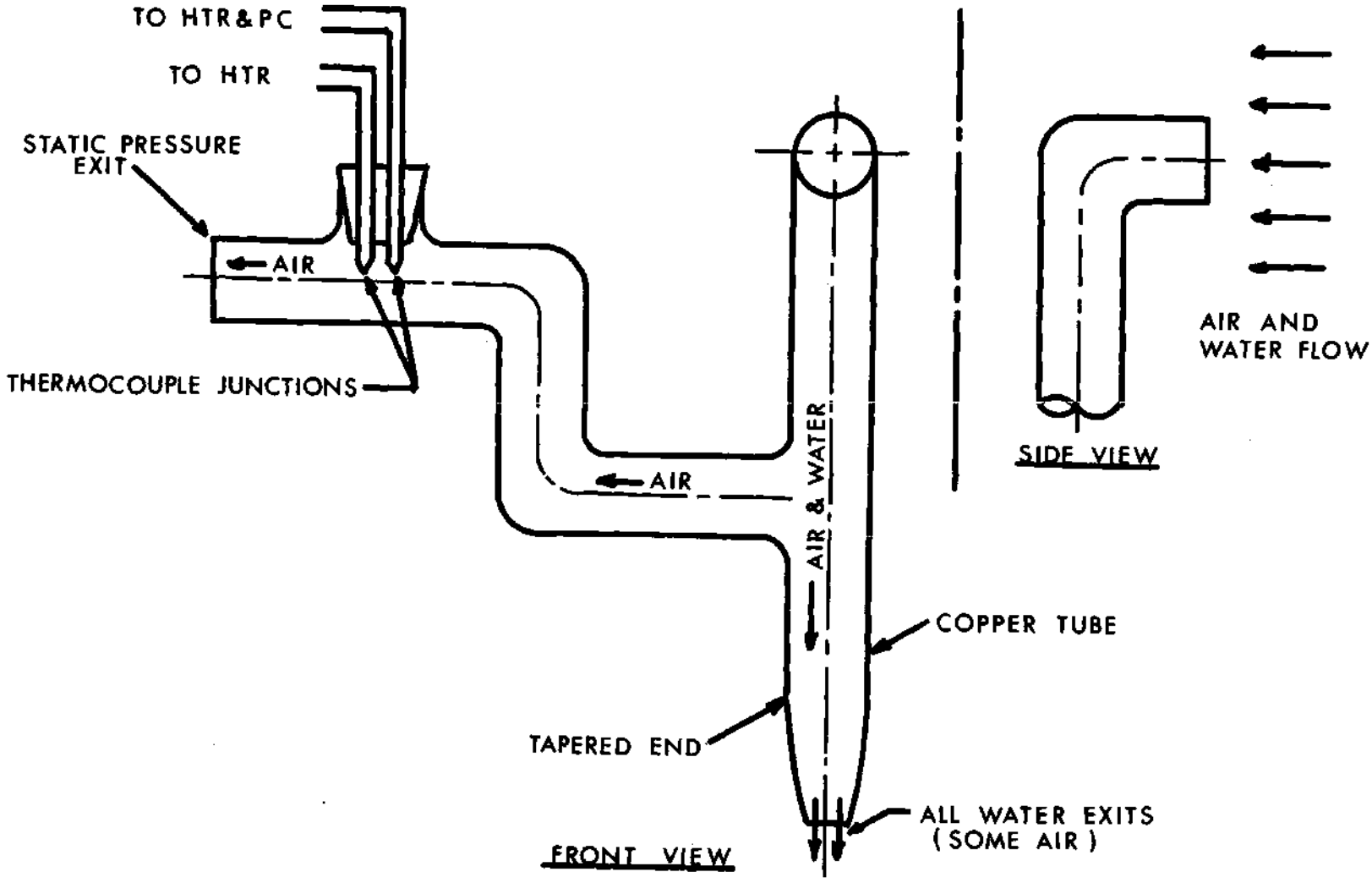

Figure 11. Air Dry Bulb Thermometer (Saterbak, Ref. 9)

bottom exit is slightly restricted, however, so some of the fluid is forced to travel up past the thermocouple and out through the upper section exit opening. The water droplets are not carried up by the small flow rate through the upper section and thus the thermocouple is exposed only to the air. Two copper-constantan (24-gage) thermocouples were used in the device--one supplied the input to the recorder-controller unit while the other was connected to the multi-point recorder. The device was positioned in the duct leading from the cooling chamber to the plenum chamber.

Although it was fairly obvious that the air would become saturated, a wet bulb thermometer was located in the duct close to the dry bulb thermometer. This wet bulb thermometer consisted of five copper-constantan thermocouples connected in parallel with the junction of each thermocouple covered with a wick which was supplied with water from a reservoir. It was felt that no precautions were necessary to separate the droplets from the air before measuring the air wet bulb temperature.

Power Input to the Heaters

In order to determine the heat loss from the cylinder it was essential that the power input to each heater be known. Twelve wattmeters (one for each heater) would be the best arrangement, but the cost and availability of quality wattmeters required that a means be devised for switching one wattmeter in and out of each heater circuit without disturbing the voltage to the heater in that circuit. The circuit used is shown in Figure 12. Using this arrangement the wattmeter could be switched from one circuit to another by flipping four switches. Since the presence of the wattmeter did have a slight effect on the voltage

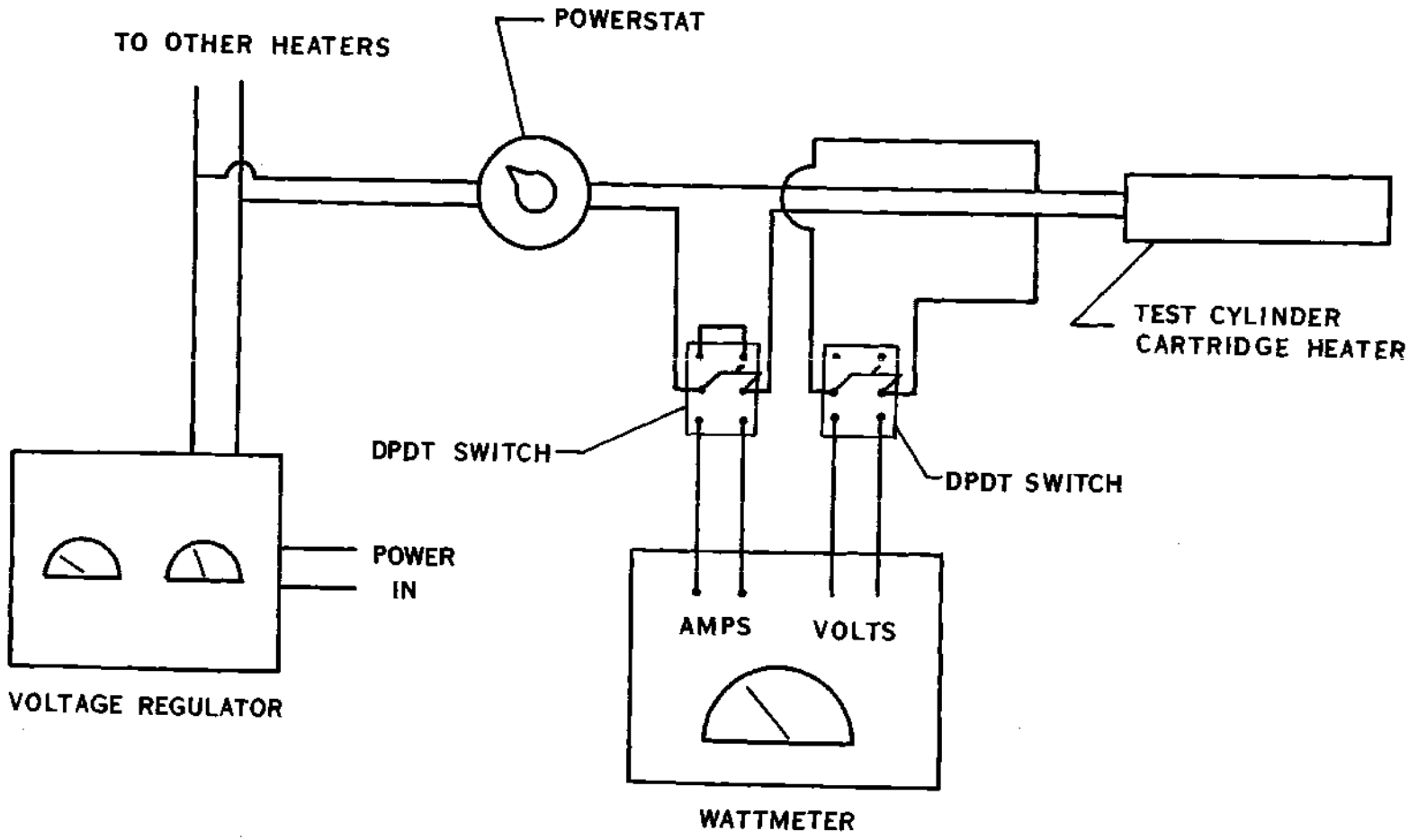

Figure 12. Electrical Circuit for Cylinder Heaters (Typical)

to the heaters, a procedure was developed to compensate for this effect while measurements were being taken (see "Procedure" section).

Air Velocity

A 0.078-inch diameter pitot tube was used to determine the air velocity in the test section. A micromanometer (least count = 0.001 inches) indicated the velocity pressure in inches of water. The air static pressure was found from the barometric pressure and the static pressure (gage) in the test section as indicated by a U-tube manometer. Air velocity data were taken with the spray turned off and it was assumed that the introduction of the spray water had a negligible effect on the air velocity.

Mass Flow Rate of Droplets

The theoretical analysis indicates that a very important parameter necessary to describe the heat transfer and hydrodynamic situation is the mass flow rate of liquid entrained in the air. A great deal of effort, therefore, went into selection of equipment and techniques from which this flow rate could be found. One very sophisticated technique involving the absorption of gamma radiation was suggested by work done by Petrick and Swanson (20). This technique, however, will yield only an "average" value across the flow area and it was also felt that the required equipment would be much too bulky and cumbersome for this study. This approach was, therefore, abandoned. Another approach reported by several investigators involves using a small tube inserted into the flow to capture a sample of the fluid. The water and air are then separated and measurement of the amount of water collected gives an indication of the droplet mass flow rate.

The latter technique was used by Alexander and Coldren (21) who studied two-phase flow in tubes. It was also recommended by Dussourd (19) who pointed out that it is necessary to maintain a flow through the collection tube if a representative sample is to be withdrawn from the main stream. The technique was also applied by Acrivos (2), Hoelscher (3), Takahara (5), and Smith (7) although none of these investigators made any attempt to maintain a flow through their probes.

A thorough experimental study of collection probes was reported by Amstead (22). He compared droplet collection rates obtained from a probe in which there was maintained a velocity equal to the velocity of the stream being sampled, with those of a probe in which only a small (ten feet per second) velocity was maintained. The results of his study showed that there was no difference between the collection rates, but a velocity had to be maintained through the probes.

Based upon Dussourd's (19) and Amstead's (22) work a system for measuring droplet flow rates was designed and built (see Figure 13). This collection system consisted of three brass pitot tubes (0.250-inch outside diameter, 0.228-inch inside diameter) which were mounted on a traverse. The end of each tube led to a graduated cylinder which acted as a plenum for collecting any liquid in the sample drawn through the tube. A second tube ran from each graduated cylinder to a static pressure tap in the side of the wind tunnel. The purpose of this second tube was to allow a continuous flow of air through the probe. When the wind tunnel was operating at low (20 feet per second) air velocities it was found that the static pressure tube had to be connected to the inlet of a small variable speed blower in order to insure the continuous

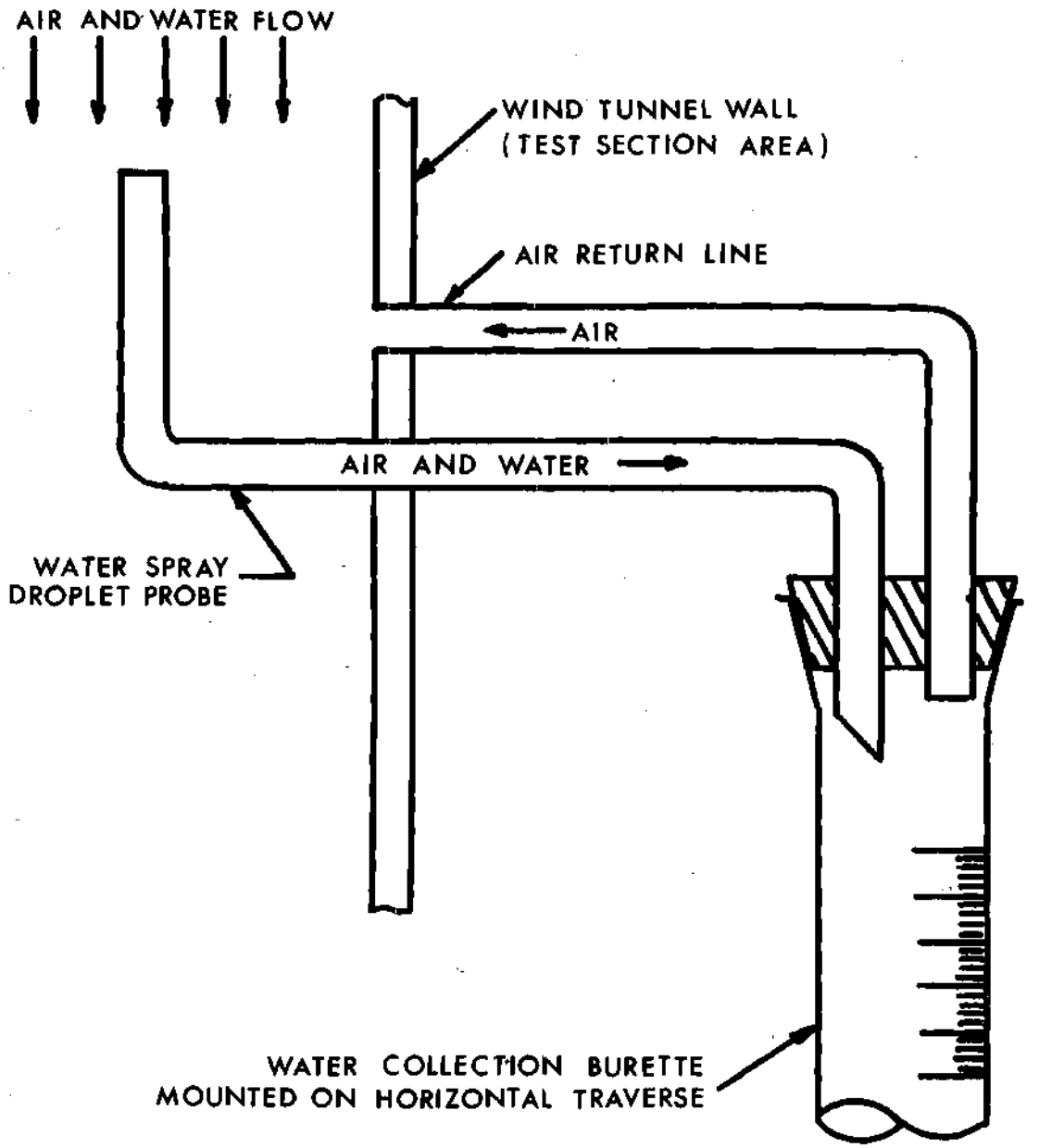

Figure 13. Droplet Mass Flow Collection Probe (Saterbak, Ref. 9)

flow of air through the probe. A small flowmeter gave an indication of the velocity obtained. An electric timer indicated the collection time.

CHAPTER IV

PROCEDURE

General

Several procedures were followed during the experimental portion of the program. These procedures involved preliminary tests on the wind tunnel, calibration of thermocouples, determination of spray distributions, and heat transfer tests. Since the analytical development indicated that the free stream air Reynolds number and the water-to-air mass flow ratio were the dependent variables involved, tests were established to check the effect of these two quantities on the heat transfer from the cylinder.

Wind Tunnel Velocity Profiles

After the wind tunnel had been assembled, it was necessary to investigate the velocity profiles that would exist in the test section due to the closed loop design. A series of pitot tube traverses were conducted at nominal air velocities of 20, 50, and 80 feet per second. The results indicated a variation of 0.5 feet per second at a nominal air velocity of 80 feet per second, while no variation was detected at nominal velocities of 50 and 20 feet per second.

Hot wire turbulence readings were also taken. These readings indicated that the turbulence level in the test section ranged from 2 per cent at 20 feet per second to 6 per cent at 80 feet per second.

Thermocouple Calibration

After the thermocouples were soldered into the cylinder surface, the brass cylinder was immersed in a Precision Scientific constant temperature bath. The thermocouples were then calibrated against a Fisher Scientific thermometer with a range from -1 to 101°C and a least count of 1/5°C. Calibration was performed from 70°F to 150°F in 10°F increments. The maximum correction for any thermocouple was 1/2°F. A similar procedure was followed for the thermocouple used to measure the air dry bulb temperature and for the thermocouple used to measure the spray water temperature.

Heat Transfer Tests

The procedure followed in obtaining heat transfer data consisted of three separate phases:

1. Establishment of a known, steady air flow through the test section.
2. Introduction of spray water and determination of the droplet flow rate.
3. Measurement of the heat flux from the cylinder at a given cylinder temperature.

The air velocities chosen for tests were 20, 50, and 80 feet per second. A pitot tube located at the top of the test section (see Figure 6) indicated the air velocity which was regulated by a damper located on the fan exhaust. The cooling water flow was regulated to maintain a steady air temperature. After the system reached steady state conditions, readings were taken of the barometric pressure, static pressure in the

test section, air velocity pressure, and air temperature (both wet and dry bulb).

After the above readings were obtained, spray was introduced into the air stream by turning on the turbine pump and adjusting the pressure regulator to provide a suitable nozzle supply pressure. The sump drain, sump heaters, and cooling water were then adjusted to maintain the air and spray temperatures to within 1°F of each other and at the same temperature (±1°F) as the air was before the spray was turned on. After steady state conditions were obtained, the droplet mass flow rate was determined.

To determine the droplet flow rate the three pitot collection probes were inserted into the air stream. After a steady collection rate was observed, the volume of water collected in 600 seconds was recorded. Fifteen readings were taken--all within the projected area of the cylinder (the 3-inch by 4-inch central area of the test section). The average of these 15 readings was taken to represent the mass flow of the droplets in the test area.

After the droplet flow rate was determined, the collection probes were removed from the test section and the cylinder heaters were turned on. It was possible to regulate the voltage applied to each heater so that the cylinder thermocouples read to within 1/2°F of each other. After steady state operation was obtained, the temperature of each thermocouple was measured with a manual potentiometer and the power input to each heater was determined. As was stated earlier, the introduction of a wattmeter into a heater circuit altered slightly (5 per cent) the voltage to the heater in that circuit. The procedure used to compensate

for this effect consisted of taking a reading of the heater voltage before introduction of the wattmeter, introducing the wattmeter into the circuit, adjusting the circuit powerstat to restore the initial voltage to the heater, reading the wattmeter, removing the wattmeter from the circuit, and finally, readjusting the powerstat to restore the original voltage to the heater. This procedure was followed, starting with the rear heaters and working forward to the front heaters.

A single heat transfer test took approximately three hours to perform. No unusual difficulties were experienced in obtaining data.

Droplet Velocities

One of the assumptions made in setting up the mathematical model was that the droplets and the air stream had the same free stream velocity approaching the cylinder. Although preliminary design of the wind tunnel was based upon research by Jenkins (23) who investigated the distance required for a droplet initially at rest to be accelerated to the velocity of the air stream it is placed in, the droplets in the present study emerged from the nozzle at a much higher velocity than the air stream. Thus, the droplets had to slow down if they were to assume the same velocity as the air and it was felt that the results of Jenkins' study might not apply directly to the present study. It was decided, therefore, that the droplet velocities should be measured experimentally. It was felt that if the droplets could be slowed down to the air velocity at the test section for the lowest air velocity used, then it could be safely assumed that the droplets would be at the same velocity as the air for greater air velocities. A program was developed for measuring the droplet velocities in the test section for

an air velocity of 20 feet per second.

Two techniques for determining the droplet velocities were investigated. The first technique, suggested by Dussourd (19) and Sucuc (24) involves measuring the increase in the velocity pressure of the fluid stream when droplets are introduced. This increase is due to the momentum of the droplets. If the velocity pressure of the two-component stream, the velocity pressure of the single component (air) stream, and the droplet mass flow rate are known, then the average droplet velocity can be calculated. This technique, however, cannot give the velocity of individual droplets and for the range of variables (stream velocity and droplet flow rates) encountered in the present study, the experimental error involved in taking the necessary data amounted to over 100 per cent. This approach was therefore abandoned.

High-speed motion pictures proved to be the best tool for determining droplet speeds. A plexiglass cylinder (3-inch diameter) with a 1-inch section removed was inserted into the test section (see Figure 14) with a thread tap (no. 0-80) positioned in the cylinder for dimensional reference. A Hy-cam high-speed motion picture camera set at 8,000 frames per second recorded the droplet trajectories as they moved through the void in the cylinder. The cut-out cylinder was used to insure that only droplets near the reference tap would be photographed. Results from the film indicated that the droplets were travelling in straight paths and it was possible to determine their velocities by noting their displacement relative to the thread tap. The time involved was calculated from the frame speed which was in turn indicated by a timing light in the camera which left small timing marks on the film

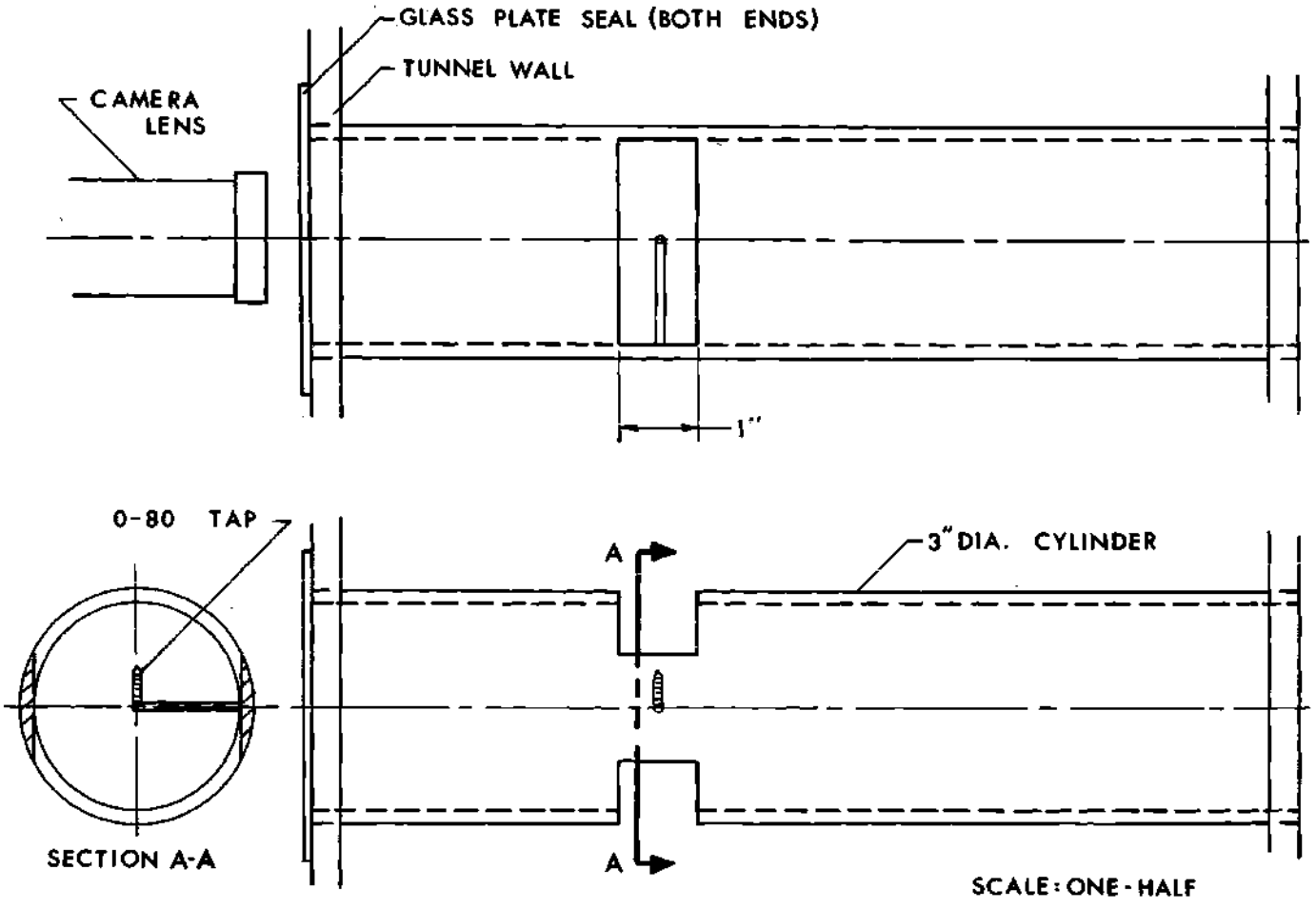

Figure 14. Photographic Arrangement for Determining Droplet Speeds

every 0.001 seconds. Velocities of 41 droplets were determined and the range was found to be from 25 to 30 feet per second. The free stream air was travelling at 20 feet per second, while the velocity of the air in the cylinder cut-out was 35 feet per second (due to the venturi effect of the cylinder in the test section).

It was felt that the above results justified the assumptions made concerning the droplet velocities and trajectories.

CHAPTER V

PRESENTATION AND DISCUSSION OF RESULTS

Introduction

As mentioned earlier, this thesis does not present all the experimental data obtained during the study. The reader is referred to Saterbak's thesis (9) for a presentation of all the experimental data generated during the program.

Figures 15, 16, and 17 compare experimentally-determined local Nusselt numbers (based upon the cylinder diameter and the thermal conductivity of water) with those predicted by Equation (18). Results are presented for free stream Reynolds numbers of from 30,000 to 118,000 and for a range of water-to-air mass flow ratios of from 1 to 6 per cent. Data for no water (air alone) are also shown in these figures. A comparison of the experimental data of Takahara (5), Smith (7), and the present study is shown in Figure 18 for a Reynolds number of 120,000 and a mass flow ratio of about 4 per cent. Smith's analytical results for the same Reynolds number are compared with those of the present study in Figure 19.

Experimental Results

General

It is obvious from Figures 15, 16, and 17 that the heat transfer from the cylinder is very sensitive to the rate at which water impinges on the surface. That is, any increase in the droplet flow rate (either

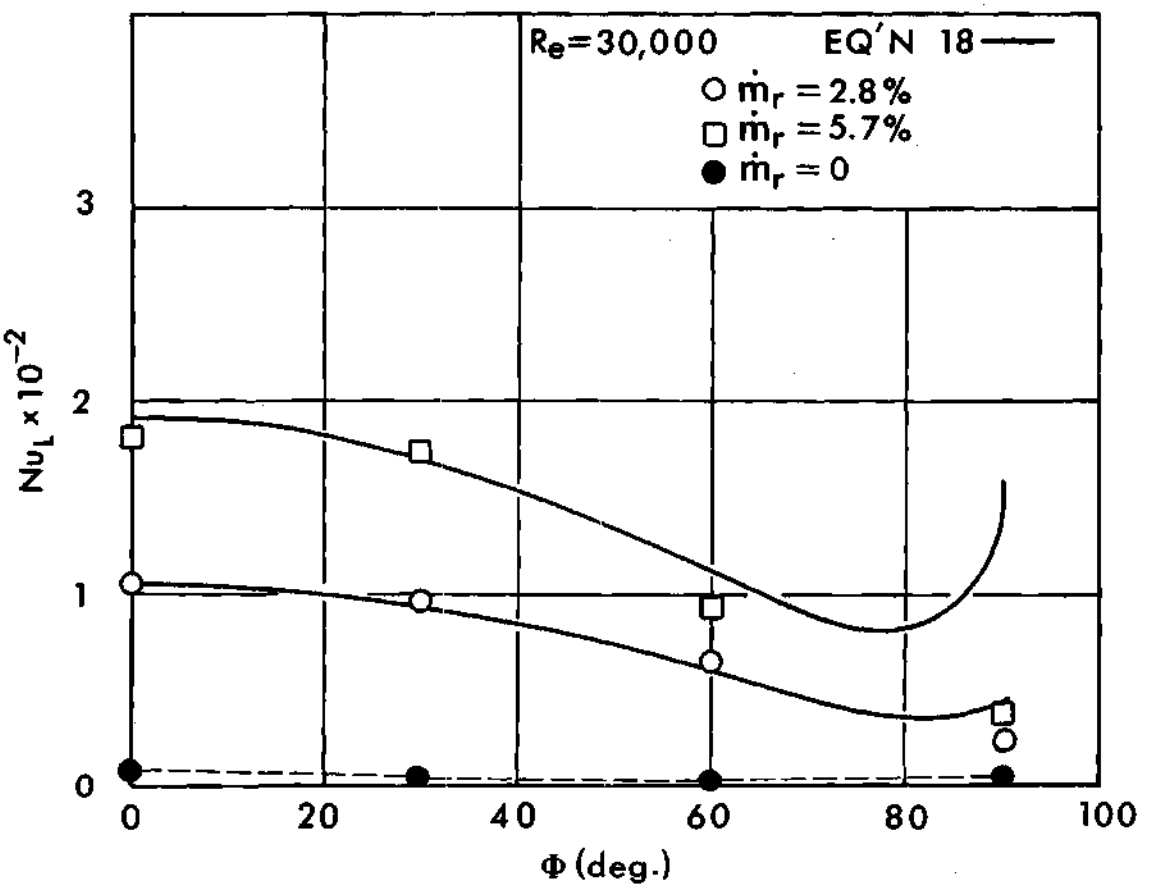

Figure 15. Comparison of Analytical and Experimental Local Nusselt Numbers for Re = 30,000

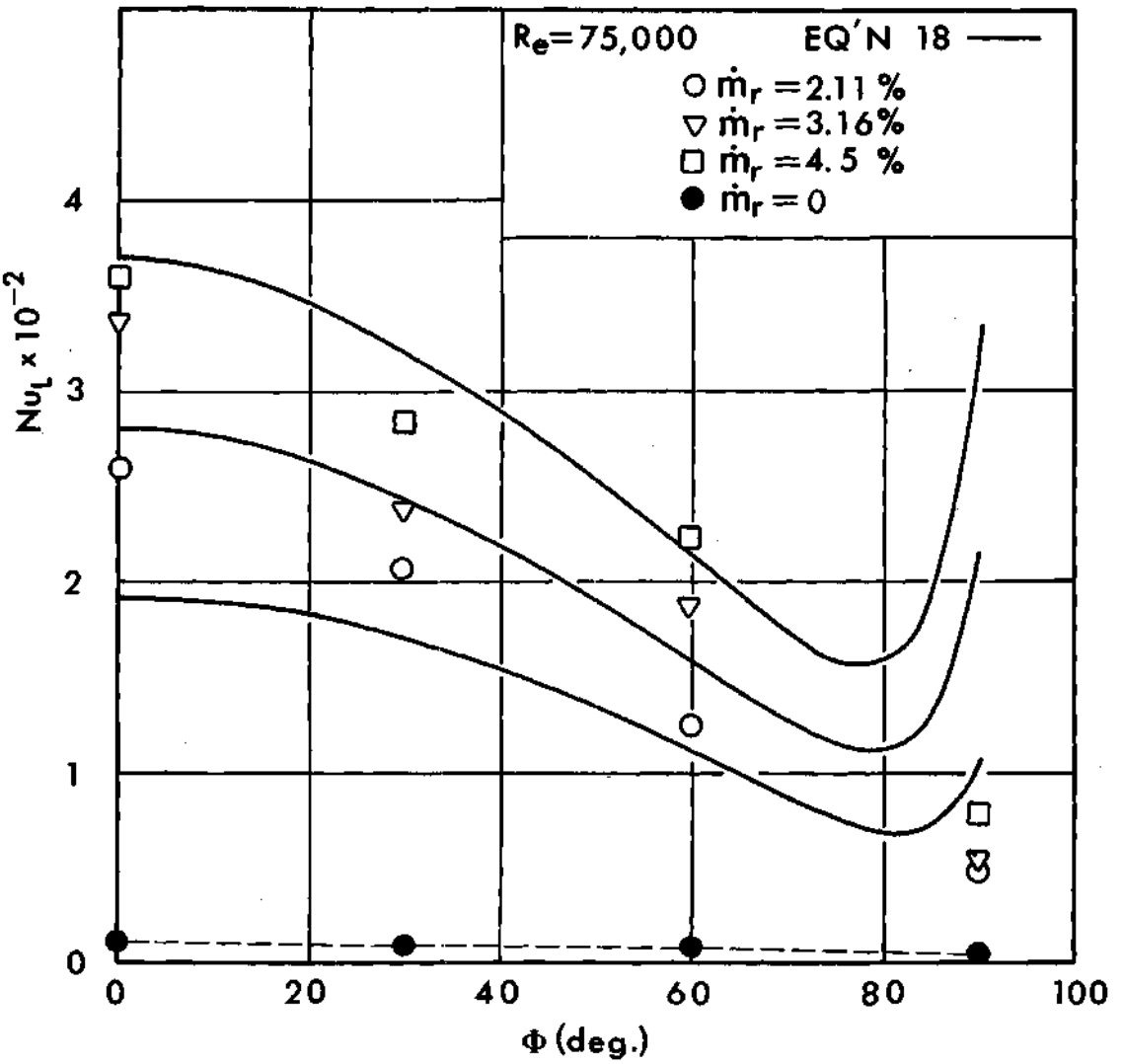

Figure 16. Comparison of Analytical and Experimental Local Nusselt Numbers for Re = 75,000

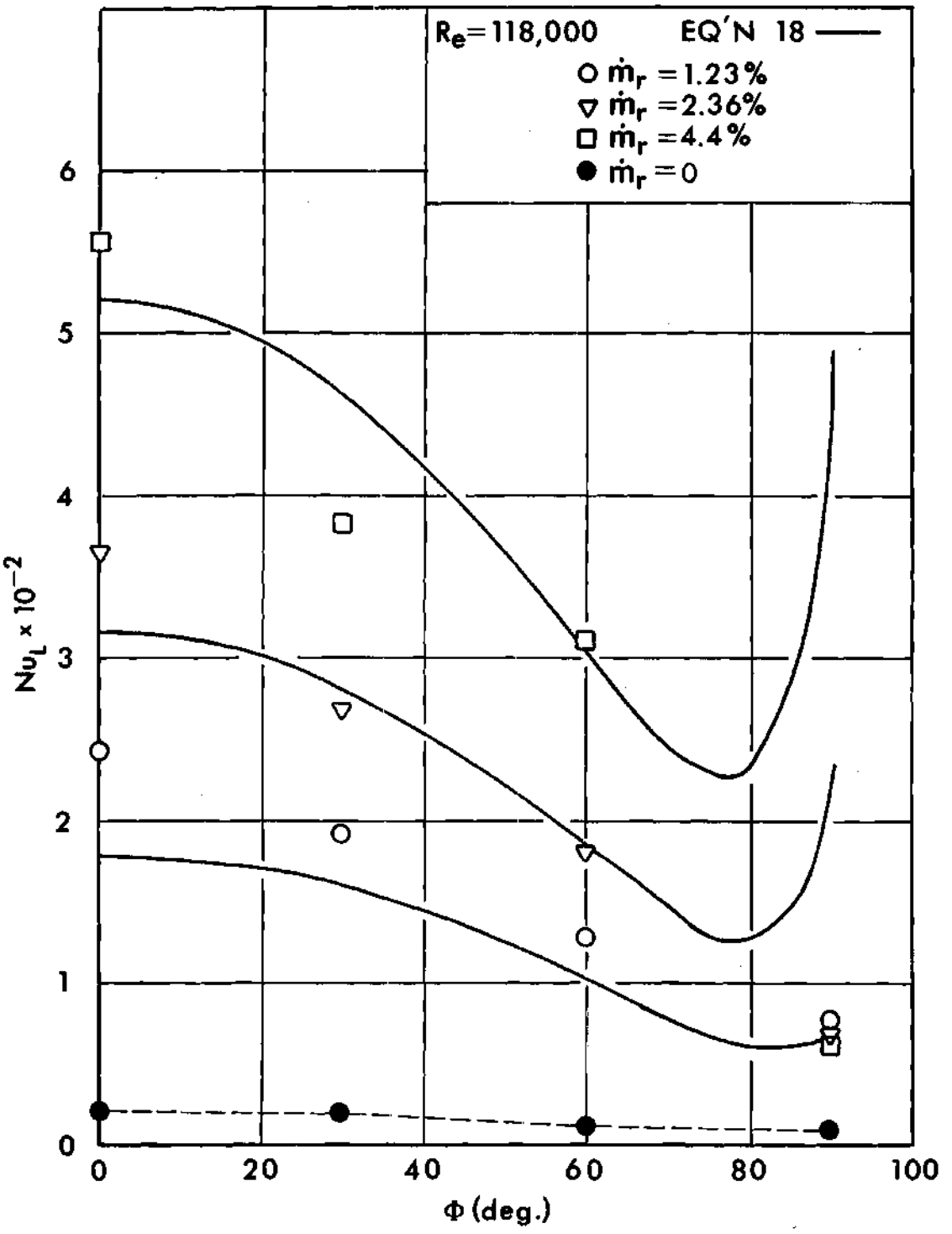

Figure 17. Comparison of Analytical and Experimental Local Nusselt Numbers for Re = 118,000

by increasing the air velocity or by spraying more water into the air) results in an increase in the Nusselt number. The increase in the local heat transfer coefficient over the front half of the cylinder is approximately the same as the ratio of the thermal conductivity of water to that of air--the reason for this being that the Nusselt number for air alone (which is based on the thermal conductivity of air) is on the same order of magnitude as the Nusselt number for spray heat transfer (which is based on the thermal conductivity of water). The dotted lines on Figures 15, 16, and 17, do not represent the analytical solution for $\dot{m}_r = 0$, but merely connect the experimental data points.

The local rate of heat transfer decreased with increasing angular displacement from the stagnation point up to 90° where it levelled out and remained essentially unchanged around the wake region. Visual observations made during the tests verified that the liquid film thickness increased rapidly near the 90° position (as could be predicted from Equation (11)) and then became unstable. The liquid ran down the rear side of the cylinder in small rivulets. Because of these small rivulets it is felt that an analysis of the wake region will be exceedingly difficult due to the uncertainty of the flow regime in that area.

A series of tests was conducted during which the temperature difference between the cylinder and the droplets was varied from 20°F to 30°F to 40°F. As the analysis predicted, the heat transfer was directly proportional to this temperature difference and no significant change in the Nusselt number resulted (see Appendix D, Table 9).

Comparison with Other Investigators

Figure 18 indicates that Takahara's (5) results differ from those of Smith (7) and the present study by a margin that is in excess of the experimental errors involved (see below). These resuls lead one to believe that there was heat conduction from Takahara's front heaters to his rear heaters. That is, part of the heat generated in the front heaters was dissipated at the rear of the cylinder. This would give the impression of high heat transfer from the front of the cylinder and low heat transfer from the rear of the cylinder. Because of the wide disagreement between Takahara's results and those of the present study, it is felt that Takahara's results are subject to question.

The data of Smith and the present study agree rather well, particularly in the wake region. The disagreement between the two studies is well within the combined experimental accuracy claimed for both studies.

Estimated Experimental Accuracy

The experimental Nusselt number is a function of several measured variables: the temperature difference, $T_o - T_\infty$; the power input to each heater, W; the air Reynolds number, Re; and the water-to-air mass flow ratio, $\dot{m}_r$. That is,

$$Nu_L = f(T_o - T_\infty, W, Re, \dot{m}_r)$$

and changes (or uncertainties) in each of the independent variables affect the Nusselt number as:

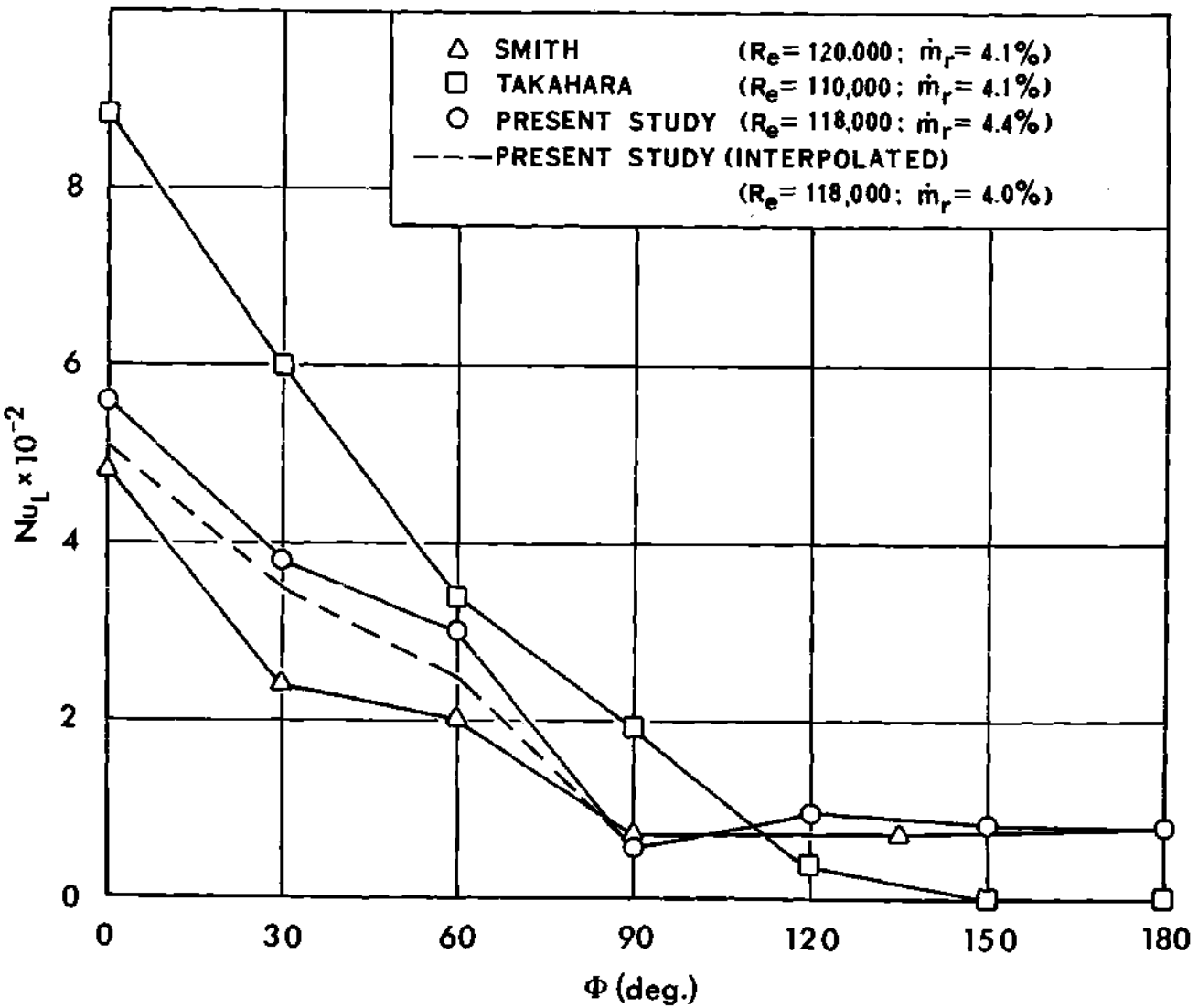

Figure 18. Comparison of Experimental Results with Those of Other Investigators

$$\frac{\Delta(Nu_L)}{Nu_L} = \frac{\partial f}{\partial(T_o - T_\infty)} \frac{\Delta(T_o - T_\infty)}{Nu_L} + \frac{\partial f}{\partial W} \frac{\Delta W}{Nu_L} + \frac{\partial f}{\partial Re} \frac{\Delta Re}{Nu_L} + \frac{\partial f}{\partial \dot{m}_r} \frac{\Delta \dot{m}_r}{Nu_L} \qquad (21)$$

The Nusselt number is directly proportional to both the temperature difference and the heater power input, so that

$$\frac{\Delta(T_o - T_\infty)}{Nu_L} \frac{\partial f}{\partial(T_o - T_\infty)} = \frac{\Delta(T_o - T_\infty)}{T_o - T_\infty} \quad ; \quad \frac{\Delta W}{Nu_L} \frac{\partial f}{\partial W} = \frac{\Delta W}{W}$$

In the present study it is felt that T_o was known to within ±1°F and T_∞ to within ±1/2°F. Thus $\Delta(T_o - T_\infty)$ is about ±3/2°F and since $T_o - T_\infty$ was about 30°F, $\frac{\Delta(T_o - T_\infty)}{T_o - T_\infty}$ is about ±0.05. The wattage was felt to be known within 1 per cent so that $\frac{\Delta W}{W}$ is about ±0.01.

The dependence of the Nusselt number on Re and $\dot{m}_r$ can only be estimated from the experimental results. These results indicate that $\frac{\partial f}{\partial Re} \frac{Re}{Nu_L}$ is about 3, and therefore since $\frac{\Delta Re}{Re}$ is felt to be within 1 per cent, $\frac{\partial f}{\partial Re} \frac{\Delta Re}{Nu_L}$ is about ±0.03. A similar analysis applied to the dependence upon the mass flow ratio indicates that $\frac{\partial f}{\partial \dot{m}_r} \frac{\dot{m}_r}{Nu_L}$ is about 0.8. Because the apparatus for determining the mass flow rate of the droplets gave consistent repeatability to within 10 per cent, it is felt that a fair estimate of $\frac{\Delta \dot{m}_r}{\dot{m}_r}$ is ±0.10. Using this figure, $\frac{\partial f}{\partial \dot{m}_r} \frac{\Delta \dot{m}_r}{Nu_L}$ is about ±0.08. If the above findings are substituted into Equation (21), the result is that $\frac{\Delta Nu_L}{Nu_L}$ = ±17 per cent.

Analytical Results

General

The analytical Nusselt numbers as obtained from Equation (18) show good agreement with those obtained experimentally. The equation breaks down at about $\phi = 80°$ because the neglected temperature derivative and body force terms become significant (see Figure 20). If the region up to 80° is considered, the maximum difference between the experimental and analytical Nusselt numbers is found to be about 25 per cent at the stagnation point for Re = 75,000 and $\dot{m}_r = 0.0211$. The analysis is not valid for $\dot{m}_r = 0$ because the basic assumption of the existence of a liquid film is not valid for a stream with no droplets in it.

Comparison with Others

Smith's (7) final equation for the local heat transfer coefficient in two-component flow contained the film thickness, δ, as one of the variables. In order to produce numerical values for the film thickness, Smith presented two simultaneous equations (one of them being a differential equation) which had to be solved. Unfortunately, Smith did not indicate how the solution to these simultaneous equations may be obtained and it was not obvious to this author how Smith obtained the analytical results he presented. As a result, Smith's theoretical solutions have not been corrected for the error contained in his final equation (see Appendix B). Smith presented his analytical findings for the stagnation point and $\phi = 30°$ only. Figure 19 compares Smith's analytical heat transfer coefficients (converted to Nusselt numbers) with those of the present study for a Reynolds number of 120,000.

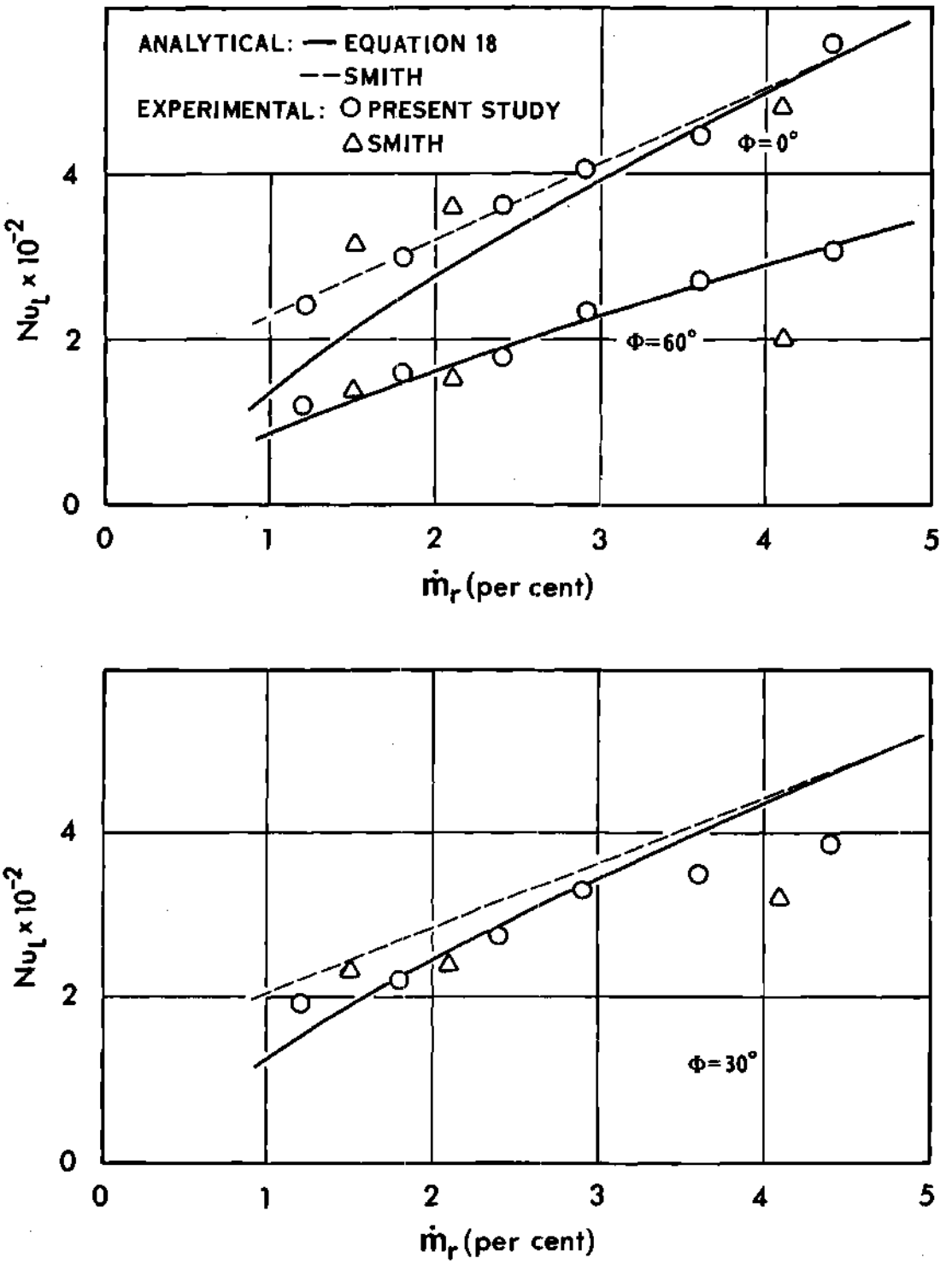

Figure 19. Comparison of Analytical Local Nusselt Numbers with Those of Smith for Re = 120,000

It is clear from Figure 19 that the experimental data are in very close agreement with Equation (18) for $\phi = 30°$ and $\phi = 60°$, but do not agree very well for low mass flow ratios at the stagnation point. No reason can be given for this behavior at the stagnation point. Smith's equation shows excellent agreement with the data at the stagnation point for all mass flow ratios.

Actually, the analytical results should be lower than the data because no consideration was given in the analysis to the disturbances which occur when the droplets enter the film. These disturbances should help to increase the heat transfer and should have their greatest effect at the stagnation point. It is felt that the unusually good agreement shown between Smith's equation and the stagnation point data is a coincidence.

Since the present analysis neglected evaporation and gave satisfactory agreement with the data, it is felt that the assumption made to neglect evaporation is verified.

The present analysis assumed "a-priori" that the thermal boundary layer extends beyond the liquid film. This assumption was justified by the analytical results which indicated that the film-air interface temperatures were closer to the cylinder temperature than that of the free stream. It seems possible, however, that enough liquid could impinge onto the cylinder to cause a film that would be thick enough to include the thermal boundary layer. It is anticipated that once this situation exists, the present analysis will not serve to describe the problem. It is also possible that once the thermal boundary layer lies inside the film, then the further addition of liquid into the air stream

may not serve to increase the heat transfer from the cylinder, but could serve to decrease it by thickening the film.

Although the above are only conjectures, they serve to indicate that the characteristics of the heat transfer system may be subject to considerable question for those values of $\dot{m}_r$ and Re beyond those studied experimentally. The reader is therefore cautioned to use care in extrapolating the results of this study.

CHAPTER VI

CONCLUSIONS AND RECOMMENDATIONS

Conclusions

The results of this study lead to several conclusions:

1. The addition of water droplets to an air stream greatly increases the heat transfer from a cylinder placed in that stream.

2. The heat transfer from a cylinder exposed to a two-component stream increases with the gas phase velocity (Reynolds number) and the water-to-air mass flow ratio, and is directly proportional to the temperature difference between the spray and the cylinder.

3. The experimental results of Smith (7) are in agreement with those of the present study, but neither agrees with the results reported by Takahara (5).

4. It is possible to predict the heat transfer from a cylinder exposed to a two-component crossflow. The equation presented is valid for the front 160 degrees of the cylinder where a major portion of the heat transfer occurs.

Recommendations

Since the front half of the cylinder has already been treated quite thoroughly, it is recommended that further studies in the field of spray heat transfer deal with the practical implementation of the results of this study.

As was previously mentioned, the present analysis yields values

for the Nusselt number which should not be extrapolated beyond the range of $\dot{m}_r$ covered experimentally. It is recommended that further experimental studies be undertaken to investigate the heat transfer which occurs when the liquid-to-air mass flow ratio is increased beyond the range covered by this study.

APPENDIX

APPENDIX A

DROPLET TRAJECTORIES AND AIR STREAMLINES

In Chapter II, two of the assumptions made in setting up the hydrodynamic portion of the problem concern the interaction between the air stream and the droplets. One assumption involves the trajectories of the droplets as they approach the cylinder, while another assumption concerns the effect droplets have in modifying the potential flow around the cylinder.

It is felt that the main criterion for judging how much effect the droplets have on the air flow is found in the relative percentages of each component present. In the experimental program that was carried out, the mass flow rates of water in the mixture amounted to less than 1/10 those of the air. In other words, $\mathring{m}_r$ was less than 10 per cent. On a volume basis, if both components were travelling at the same velocity, the percentage of the total volume occupied by the water droplets would be less than 0.01 per cent. The presence of such a small volume of water is felt to have a negligible effect on the normal airflow around the cylinder.

Consideration of the trajectories of droplets in the air stream is aided greatly by the research which has been directed toward the problem of aircraft wing icing. An excellent review of the literature pertaining to droplet trajectories is found in reference 25. Brun et al. (26) reported droplet trajectories as determined by a mechanical

analog and presented charts from which it is possible to estimate what percentage of the droplets will be intercepted by the cylinder and what percentage will be swept away from the cylinder by the air flow. For the droplet size distribution supplied by the nozzle manufacturer, more than 90 per cent of the smallest 10 per cent of the droplets would hit the cylinder according to Brun's calculations. Since the larger droplets have straighter trajectories, they too would hit the cylinder. The droplet trajectories are, therefore, essentially straight. The simplification obtained by assuming straight trajectories is that one is not faced with a numerical solution before the film is even considered.

APPENDIX B

CONSIDERATION OF EVAPORATION EFFECTS

One of the assumptions made in developing the energy equation was that evaporation from the film may be neglected. Since the edge of the film is heated to a temperature higher than the free stream temperature, a potential for evaporation will exist and it is essential that the assumption be justified by means other than intuitive reasoning.

If the local evaporation rate per unit area from the film, $\dot{m}''_{evap}$, is known, then the heat transfer required to evaporate this mass is given by:

$$\dot{q}_{evap} = \dot{m}''_{evap} h_{fg}$$

where $\dot{q}_{evap}$ is the heat transfer rate per unit area due to evaporation of liquid from the film, and h_{fg} is the enthalpy of evaporation for the liquid at the temperature of evaporation.

The evaporation rate, $\dot{m}''_{evap}$, is generally expressed in terms of a mass transfer coefficient, k_g, multiplied by some driving force for mass transfer, B. That is, $\dot{m}''_{evap} = k_g B$. Smith (7) used the approach followed by Spalding (27) in which B involves the difference between the mass fraction of water vapor in the free stream and the mass fraction of water vapor in the air adjacent to the liquid film. Other authors,

Kreith (15) in particular, choose to define k_g and B in such a manner that B involves the difference between the partial pressure of the water vapor in the free stream and the partial pressure of the water vapor next to the film. The two approaches are obviously similar because the mass fraction of water vapor is related to its partial pressure. The partial pressure approach is used in the following discussion.

The mass transfer rate per unit area is given by

$$\dot{m}''_{evap} = k_g(p_{vi} - p_{v\infty})$$

where p_{vi} is the partial pressure of the water vapor at the air-film interface and $p_{v\infty}$ is the partial pressure of the water vapor in the free stream. Calling upon the analogy between heat and mass transfer, it may be shown that the mass transfer coefficient, k_g, is related to the heat transfer coefficient for air alone flowing over a dry cylinder, h_a, by

$$k_g = \left(\frac{h_a}{\rho_a c_{pa}}\right)\left(\frac{P}{R_v T_a p_{am}}\right) Le^{\frac{2}{3}} \qquad (22)$$

where ρ_a is the air density, c_{pa} is the constant pressure specific heat of air, p is the total static pressure in the free stream, R_v is the gas constant for water vapor, T_a is the mean temperature between film and the free stream, p_{am} is the logarithmic mean partial pressure of the air defined as

$$p_{am} = \frac{p_{ai} - p_{a\infty}}{\ln \frac{p_{ai}}{p_{a\infty}}}$$

and Le is the Lewis number which is defined as the Prandtl number divided by the Schmidt number for air. As Kreith points out, for dilute mixtures (water vapor in air) $p_{am} \approx p$ so that Equation (22) becomes

$$k_g = \frac{h_a}{\rho_a c_{pa}} \frac{1}{R_v T_a} Le^{\frac{2}{3}}$$

The expression for $\dot{q}_{evap}$ is then

$$\dot{q}_{evap} = \frac{h_a}{\rho_a c_{pa}} \frac{h_{fg}}{R_v T_a} (p_{vi} - p_{v\infty}) Le^{\frac{2}{3}} \qquad (23)$$

It is possible to define a heat transfer coefficient for evaporation as

$$h_{evap} = \frac{\dot{q}''_{evap}}{T_o - T_\infty}$$

so that

$$\frac{h_{evap}}{h_a} = \left(\frac{h_{fg}}{\rho_a c_{pa} R_v T_a}\right)\left(\frac{p_{vi} - p_{v\infty}}{T_o - T_\infty}\right) Le^{\frac{2}{3}} \qquad (24)$$

In the present study the free stream air had a relative humidity very close to 100 per cent. In this case $p_{v\infty}$ becomes the saturation pressure of water vapor corresponding to the free stream temperature, T_∞, while

p_{vi} is the saturation pressure corresponding to the temperature at the edge of the film, $T_i = T_\delta$. In order to make a high estimate as to the evaporation rate and to facilitate computation, let $T_\delta = T_o$ so that p_{vi} is evaluated at T_o (this will yield values for p_{vi} higher than those which actually exist and the resulting analysis should over-estimate the effects of evaporation). For the range of temperatures considered experimentally

$$\frac{p_{vo} - p_{v\infty}}{T_o - T_\infty} \tilde{=} 0.04 \frac{lb_f}{in^2 - {}^\circ R}$$

The following numerical values were used to evaluate the other terms in Equation (24):

$$h_{fg} = 1040 \text{ Btu/lb}_m$$

$$\rho_a = 0.073 \text{ lb}_m/\text{ft}^3$$

$$c_{pa} = 0.24 \text{ Btu/lb}_m\text{-}^\circ R$$

$$R_v = 85.76 \text{ ft-lb}_f/\text{lb}_m\text{-}^\circ R$$

$$T_a = 560^\circ R$$

$$Le = 1.2$$

These values, when substituted into Equation (24), show that $h_{evap} \tilde{=} 6\, h_a$. Earlier it has been shown that the influence of convection (h_a) from the film was negligible (of order $\bar{\delta}$) compared to the sensible heating of the film (of order unity). Since evaporation heat transfer amounts to only six times that of convection from the film, it follows

that it should also be negligible. Experimental results verify this assumption in that good agreement is indicated between them and the analysis (which neglects convection and evaporation).

The equation used by Smith (7) to calculate the evaporative heat transfer rate is similar to Equation (24) except that due to a typographical error in Spalding's book, the exponent on the Lewis number is given as $-\frac{2}{3}$ instead of $+\frac{2}{3}$. The error introduced by this oversight is not very great because the Lewis number is close to unity and the evaporative heat transfer is only a small portion of the total heat transfer.

APPENDIX C

CONSIDERATION OF THE NEGLECTED DERIVATIVES IN THE ENERGY EQUATION

In Chapter II it was found that neglecting the derivative term in Equation (17) resulted in an equation which was easily solved for the temperature at the edge of the film, θ_δ. Although it is fairly obvious that the neglected term is small, so are the other terms in the equation and it is difficult to get an estimation of their relative magnitudes without resorting to a numerical investigation of each case.

One technique which has been applied to the solution of problems of this type (28) is called the method of successive approximations. This method involves neglecting the derivative term and then solving the resulting non-differential equation for the required dependent variable. This first approximation is then used to evaluate the neglected derivative term which is substituted back into the original equation. The resulting equation may then be solved for the dependent variable again, yielding the second generation or second approximation solution. The procedure is continued until the n'th approximation is felt to yield valid results.

The obvious disadvantage of the technique is that each successive approximation generally yields a much more complex expression than its predecessor.

Equation (18), therefore, represents the first approximation to

the solution of Equation (17). In order to get the second approximation, Equation (18) was differentiated with respect to ϕ. The resulting long algebraic expression for the derivative of θ_δ was substituted into Equation (17) for the neglected derivative. When the resulting equation was solved for the range of variables encountered in the experimental program, changes of less than 5 per cent were obtained between the first and second approximations. This was taken as an indication that the neglected derivative term did indeed represent a secondary effect and could be ignored.

An additional check on the validity of the approximation was obtained by a numerical integration of Equation (17). The results of the first approximation, second approximation, and numerical integration are shown in Figure 20 for one set of variables.

Heat conduction in the ϕ-direction was also neglected in the derivation of the energy equation. There are two arguments that may be used to justify this assumption. The first argument relies upon the discussion above in which it was demonstrated that the temperature gradient in the ϕ-direction was very small compared to the other terms in the energy equation and could be neglected. Since the first derivative of θ_δ with respect to ϕ is small, it follows that the second derivative (which represents ϕ-conduction) will also be small (because θ_δ is a monotonically decreasing function) and should be negligible. The second (and more forceful) argument relies upon the standard boundary-layer order of magnitude analysis which shows that the temperature gradient in the ϕ-direction is of order δ compared to the temperature derivative in the r-direction.

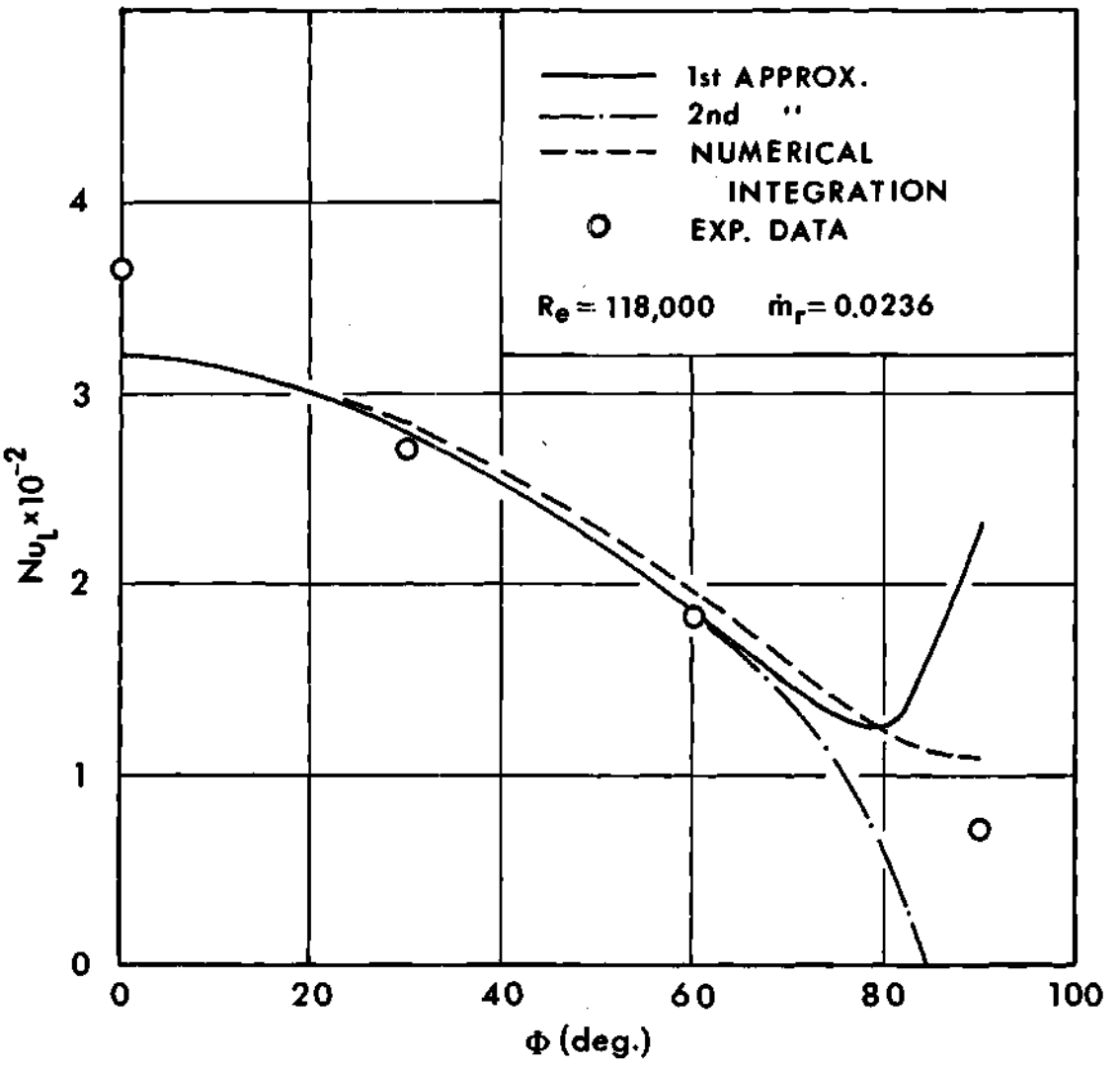

Figure 20. Comparison of Various Solutions to the Energy Equation

APPENDIX D

TABULATED HEAT TRANSFER RESULTS

The following tables present the heat transfer data as obtained from the experiments performed. Only those runs which were presented in Figures 15, 16, and 17 are given in tabular form. The reader is once again referred to Saterbak's thesis (9) for presentation of the rest of the results. Table 9 presents the data which were obtained when the cylinder temperature was varied in order to investigate the effect of various temperature differences on the Nusselt number.

The tests are numbered in accordance with the notation used by Saterbak. The "AW" or "A" prefix means that the test was run under two-component (air-water) or one-component (air) conditions, respectively; the second term (20, 50, or 80) represents the air velocity used in feet per second (Re = 30,000; 75,000 and 118,000, respectively); and the last digit identifies the particular test but has no physical significance.

Table 1. Heat Transfer in Two-Component (Air-Water) Flow

Test No. AW-20-1

Reynolds Number: 30,000

Water-Air Mass Flow Rate Ratio: 0.028

Average Water Mass Flow Rate: 0.0395 lbm/ft^2-sec
Spray Droplet Distribution Variation: ± 24%
Approximate Median Water Droplet Diameter: 230 microns
Nozzle: 1 SQ-10
Operating Pressure: 60 psig

Spray Water Temperature (T_∞): 78.0°F
Air Dry Bulb Temperature: 78.0°F
Relative Humidity: 93%

ϕ degrees	T_o °F	$T_o - T_\infty$ °F	Heat Flux BTU/hr.ft.^{2}	Nu_L Local Nusselt Number
0	111.3	33.3	5,035	108
30	110.8	32.8	4,440	96
330	111.3	33.3	5,840	121
60	111.0	33.0	3,080	66
300	111.7	33.7	2,970	61
90	111.3	33.3	1,125	24
270	110.6	32.6	1,140	24
120	111.3	33.3	1,030	22
240	111.5	33.5	1,205	25
150	111.0	33.0	2,050	44
210	111.5	33.5	1,920	40
180	111.5	33.5	2,050	43

Table 2. Heat Transfer in Two-Component (Air-Water) Flow

Test No. AW-20-3

Reynolds Number: 30,000

Water-Air Mass Flow Rate Ratio: 0.057

Average Water Mass Flow Rate: 0.0805 lbm/ft^2-sec
Spray Droplet Distribution Variation: ± 12%
Approximate Median Water Droplet Diameter: 120 microns
Nozzle: 1 SQ-10
Operating Pressure: 200 psig

Spray Water Temperature (T_∞): 79.5°F
Air Dry Bulb Temperature: 78.0°F
Relative Humidity: 93%

ϕ degrees	T_o °F	$T_o - T_\infty$ °F	Heat Flux BTU/hr.ft.^{2}	Nu_L Local Nusselt Number
0	110.2	30.7	7,730	180
30	110.2	30.7	6,090	141
330	109.8	30.3	7,770	177
60	110.1	30.6	3,740	87
300	110.4	30.9	4,075	91
90	110.3	30.8	1,530	36
270	109.0	29.5	1,060	24
120	110.0	30.5	1,220	28
240	110.2	30.7	1,000	23
150	110.2	30.7	2,455	57
210	110.2	30.7	1,080	24
180	110.6	31.1	1,890	43

Table 3. Heat Transfer in Two-Component (Air-Water) Flow

Test No. AW-50-2

Reynolds Number: 75,000

Water-Air Mass Flow Rate Ratio: 0.021

Average Water Mass Flow Rate: 0.075 lbm/ft^2-sec
Spray Droplet Distribution Variation: ± 33%
Approximate Median Water Droplet Diameter: 175 microns
Nozzle: 1 SQ-10
Operating Pressure: 100 psig

Spray Water Temperature (T_∞): 82.5°F
Air Dry Bulb Temperature: 80.0°F
Relative Humidity: 96%

ϕ degrees	T_o °F	$T_o - T_\infty$ °F	Heat Flux BTU/hr.ft.^{2}	Nu_L Local Nusselt Number
0	111.5	29.0	10,780	264
30	111.7	29.2	8,620	210
330	111.4	28.9	11,550	285
60	111.7	29.2	5,210	127
300	112.0	29.5	5,880	142
90	112.0	29.5	2,340	56
270	110.9	28.4	1,562	39
120	112.1	29.6	718	17
240	111.8	29.3	1,470	36
150	112.3	29.8	3,440	82
210	111.5	29.0	2,060	51
180	111.8	29.3	4,410	107

Table 4. Heat Transfer in Two-Component (Air-Water) Flow

Test No. AW-50-4

Reynolds Number: 75,000

Water-Air Mass Flow Rate Ratio: 0.0316

Average Water Mass Flow Rate: 0.110 lbm/ft^2-sec
Spray Droplet Distribution Variation: ± 40%
Approximate Median Water Droplet Diameter: 255 microns
Nozzle: 2 SQ-10
Operating Pressure: 50 psig

Spray Water Temperature (T_∞): 82.0°F
Air Dry Bulb Temperature: 81.2°F
Relative Humidity: 92%

ϕ degrees	T_o °F	$T_o - T_\infty$ °F	Heat Flux BTU/hr.ft.^{2}	Nu_L Local Nusselt Number
0	111.7	29.7	14,050	337
30	111.7	29.7	9,970	237
330	111.9	29.9	11,050	263
60	111.9	29.9	8,900	211
300	112.1	30.1	8,120	192
90	112.1	30.1	2,100	49
270	112.1	30.1	1,910	45
120	111.5	29.5	3,380	81
240	112.1	30.1	3,620	85
150	112.1	30.1	3,620	85
210	112.1	30.1	2,625	62
180	112.1	30.1	3,530	83

Table 5. Heat Transfer in Two-Component (Air-Water) Flow

Test No. AW-50-5

Reynolds Number: 75,000

Water-Air Mass Flow Rate Ratio: 0.045

Average Water Mass Flow Rate: 0.158 lbm/ft^2-sec
Spray Droplet Distribution Variation: ± 45%
Approximate Median Water Droplet Diameter: 210 microns
Nozzle: 2 SQ-10
Operating Pressure: 70 psig

Spray Water Temperature (T_∞): 81.0°F
Air Dry Bulb Temperature: 80.5°F
Relative Humidity: 92%

ϕ degrees	T_o °F	$T_o - T_\infty$ °F	Heat Flux BTU/hr.ft.^{2}	Nu_L Local Nusselt Number
0	110.0	29.0	14,680	360
30	109.5	28.5	9,680	241
330	109.5	28.5	11,400	284
60	109.5	28.5	9,060	226
300	110.0	29.0	8,440	206
90	110.5	29.5	3,230	78
270	110.5	29.5	2,110	51
120	109.5	28.5	3,400	85
240	109.0	28.0	3,220	83
150	110.0	29.0	3,440	84
210	110.5	29.5	3,440	83
180	110.0	29.0	3,590	88

Table 6. Heat Transfer in Two-Component (Air-Water) Flow

Test No. AW-80-1

Reynolds Number: 118,000

Water-Air Mass Flow Rate Ratio: 0.0123

Average Water Mass Flow Rate: 0.070 lbm/ft^2-sec
Spray Droplet Distribution Variation: ± 45%
Approximate Median Water Droplet Diameter: 175 microns
Nozzle: 1 SQ-10
Operating Pressure: 100 psig

Spray Water Temperature (T_∞): 79.2°F
Air Dry Bulb Temperature: 78.0°F
Relative Humidity: 90%

ϕ degrees	T_o °F	$T_o - T_\infty$ °F	Heat Flux BTU/hr.ft.^{2}	Nu_L Local Nusselt Number
0	108.9	29.7	10,180	244
30	108.0	28.8	7,810	193
330	108.9	29.7	10,100	242
60	108.0	28.8	5,310	131
300	109.1	29.9	6,120	145
90	109.0	29.8	3,320	79
270	109.0	29.8	2,780	66
120	108.3	29.1	2,340	59
240	109.8	30.6	2,810	66
150	109.1	29.9	3,590	85
210	109.0	29.8	2,960	71
180	109.4	30.4	4,060	95

Table 7. Heat Transfer in Two-Component (Air-Water) Flow

Test No. AW-80-3

Reynolds Number: 118,000

Water-Air Mass Flow Rate Ratio: 00236

Average Water Mass Flow Rate: 0.135 lbm/ft^2-sec
Spray Droplet Distribution Variation: ± 30%
Approximate Median Water Droplet Diameter: 115 microns
Nozzle: 1 SQ-10
Operating Pressure: 224 psig

Spray Water Temperature (T_∞): 77.3°F
Air Dry Bulb Temperature: 77.0°F
Relative Humidity: 95%

ϕ degrees	T_o °F	$T_o - T_\infty$ °F	Heat Flux BTU/hr.ft.^{2}	Nu_L Local Nusselt Number
0	107.6	30.3	15,620	366
30	107.6	30.3	11,470	269
330	107.2	29.9	15,480	372
60	107.3	30.0	6,660	158
300	108.3	31.0	7,940	182
90	107.3	30.0	3,000	71
270	105.4	28.1	1,750	44
120	107.3	30.0	3,120	74
240	107.1	29.8	3,720	89
150	107.2	29.9	4,840	115
210	107.3	30.0	3,530	84
180	107.3	30.0	5,590	132

Table 8. Heat Transfer in Two-Component (Air-Water) Flow

Test No. AW-80-6

Reynolds Number: 118,000

Water-Air Mass Flow Rate Ratio: 0.044

Average Water Mass Flow Rate: 0.249 lbm/ft^2-sec
Spray Droplet Distribution Variation: ± 17%
Approximate Median Water Droplet Diameter: 145 microns
Nozzle: 2 SQ-10
Operating Pressure: 140 psig

Spray Water Temperature (T_∞): 79.7°F
Air Dry Bulb Temperature: 80.3°F
Relative Humidity: 90%

ϕ degrees	T_o °F	$T_o - T_\infty$ °F	Heat Flux BTU/hr.ft.^{2}	Nu_L Local Nusselt Number
0	108.8	29.1	22,800	557
30	108.5	28.8	14,980	370
330	108.7	29.0	15,620	384
60	108.4	28.7	12,520	310
300	108.5	28.8	10,550	260
90	108.7	29.0	2,500	61
270	108.5	28.8	1,875	46
120	108.7	29.0	4,090	100
240	108.7	29.0	4,720	106
150	109.1	29.4	3,650	88
210	109.4	29.7	3,500	84
180	109.1	29.4	4,220	102

Table 9. Heat Transfer in Two-Component (Air-Water) Flow

Test No. AW-50-7

Reynolds Number: 75,000

Water-Air Mass Flow Rate Ratio: 0.058

Spray Water Temperature (T_∞): 79.3°F, 80.1°F, 81.0°F

Air Dry Bulb Temperature: 80.5°F

Relative Humidity: 90%

Average Water Mass Flow Rate: 0.206 lbm/ft^2-sec

Spray Droplet Distribution Variation: ± 41%

Approximate Median Water Droplet Diameter: 175 Microns

Nozzle: 2 SQ-10

Operating Pressure: 100 psig

ϕ degrees	$T_o - T_\infty$ °F Runs			Heat Flux BTU/hr.ft.^{2} Runs			Nu_L Local Nusselt Number Runs		
	A	B	C	A	B	C	A	B	C
0	20.8	31.8	43	9,120	14,250	20,300	312	318	340
30	20.7	32.0	43	6,275	9,470	14,850	216	228	245
330	21.5	32.0	43	8,070	12,050	17,000	266	268	280
60	20.8	32.4	43	5,030	8,720	12,300	180	185	203
300	20.8	31.8	43	5,150	8,470	12,450	177	188	206
90	21.1	32.9	43	1,435	2,160	2,830	48	47	47
270	21.1	32.0	43	1,220	1,655	2,060	41	37	34
120	20.4	32.0	43	1,940	3,440	4,375	68	76	73
240	20.0	31.6	43	2,250	4,400	5,000	80	99	83
150	20.7	32.9	43	1,940	3,910	5,470	66	85	90
210	20.7	32.0	43	1,910	3,060	3,750	66	68	62
180	20.9	31.6	43	1,910	3,750	7,810	65	85	129

Table 10. Heat Trensfer in One-Component (Air) Flow

Test No. A-20-1

Reynolds Number: 30,000

Air Dry Bulb Temperature (T_∞): 71.0°F

Relative Humidity: 97%

ϕ degrees	T_o °F	$T_o - T_\infty$ °F	Heat Flux BTU/hr.ft.^{2}	Nu_A Local Nusselt Number
0	124.5	53.5	516	157
30	124.4	53.3	352	108
60	124.0	53.0	430	132
90	124.4	53.4	281	85
120	124.4	53.4	156	47
150	124.0	53.0	742	228
180	124.3	53.3	828	252
210	124.2	53.2	735	224
240	124.4	53.4	296	90
270	124.3	53.3	195	59
300	124.8	53.8	375	113
330	123.7	52.7	600	185

Table 11. Heat Transfer in One-Component (Air) Flow

Test No. A-50-1

Reynolds Number: 75,000

Air Dry Bulb Temperature (T_∞): 74.3°F

Relative Humidity: 98%

ϕ degrees	T_o °F	$T_o - T_\infty$ °F	Heat Flux BTU/hr.ft.^{2}	Nu_A Local Nusselt Number
0	115.7	41.4	655	256
30	115.7	41.4	469	183
60	115.3	41.0	430	170
90	115.9	41.6	469	183
120	115.9	41.6	274	107
150	115.4	41.1	968	382
180	115.8	41.5	1,015	396
210	115.4	41.1	945	374
240	115.4	41.1	382	151
270	115.5	41.2	312	122
300	116.0	41.7	516	200
330	114.8	40.5	664	266

Table 12. Heat Transfer in One-Component (Air) Flow

Test No. A-80-1

Reynolds Number: 118,000

Air Dry Bulb Temperature (T_∞): 76.9°F

Relative Humidity: 96%

ϕ degrees	T_o °F	$T_o - T_\infty$ °F	Heat Flux BTU/hr.ft.^{2}	Nu_A Local Nusselt Number
0	117.1	40.2	1,210	489
30	116.9	40.0	734	297
60	117.1	40.2	734	296
90	117.5	40.6	780	312
120	117.3	40.4	718	289
150	116.9	40.0	1,258	510
180	117.3	40.4	1,367	548
210	116.7	39.8	1,220	497
240	116.5	39.6	750	307
270	116.5	39.6	648	263
300	117.5	40.6	804	322
330	115.3	38.4	1,093	461

APPENDIX E

DETAILS OF EQUIPMENT USED

Wind Tunnel Fan

Capacity: 6,000 c.f.m. at 7 inches of water pressure

Manufacturer: Industrial Division of American Standard, Detroit, Michigan

Model: Series 106, Type E, Size 17

Drive: 15-horsepower electric motor ("V"-belt drive)

Pitot Tube Manometer

Description: Micromanometer, 10-inch capacity, 0.001-inches least count.

Manufacturer: Meriam Instrument Company, Cleveland, Ohio

Model: 34FB2

Hot Wire Anemometer

Description: Flow Corporation Models 12A1 and HWB

Potentiometer

Description: Leeds and Northrup Model 8686

Wattmeter

Description: Weston Model No. 310, least count 1 watt, factory calibrated to within 0.3 watts

Spray Pump

Description: Single-stage turbine pump

Manufacturer: Aurora Pump Company

Model: TS-EST-1

Cylinder Heaters

Description: "Firerod" 0.375-inch diameter by 4-inch long cartridge heaters (125, 250, and 500 watts at 115 volts)

Manufacturer: Whatlow Electric Manufacturing Co., St. Louis, Missouri

Heater Power Supply

Description: Voltage regulator (variation within 0.01 per cent)

Manufacturer: Sorensen and Company, Inc., South Norwalk, Connecticut

Model: No. 2501

Reference Thermometer for Thermocouple Calibrations

Description: Mercury-in-glass thermometer, -1 to 101°C range, least count 0.2°C

Manufacturer: Fisher Scientific Co.

Model: No. 15-043-C

Recorders and Controllers

Both the recorder-controller and the multi-point recorder were originally custom-built by Honeywell for Georgia Institute of Technology.

LITERATURE CITED

1. Elperin, I. T., "Heat Transfer of Two-Phase Flow with a Bundle of Tubes," *Inzhererno-Fizicheski Zhurnal,* Vol. IV, No. 8, pp. 30-35, August, 1961.

2. Acrivos, A., J. E. Ahern, and A. R. Nagy, Jr., *Research Investigation of Two-Component Heat Transfer,* The Marquardt Corporation, ARL Report ARL 64-116, Wright-Patterson AFB, Ohio, June, 1964.

3. Hoelscher, F., *Study of Heat Transfer from a Heated Cylinder in Two-Phase, Water-Air Flow,* Master's Thesis, Air Force Institute of Technology, Wright-Patterson AFB, Ohio, March, 1965.

4. Tifford, A. N., *Explanatory Investigation of Laminar Boundary Layer Heat Transfer Characteristics of Gas Liquid-Spray Systems,* Ohio State University Research Foundation, ARL Report ARL 64-136, Wright-Patterson AFB, Ohio, September, 1964.

5. Takahara, E. W., *Experimental Study of Heat Transfer from a Heated Circular Cylinder in Two-Phase, Water-Air, Flow,* Master's Thesis, Air Force Institute of Technology, Wright-Patterson AFB, Ohio, March, 1966.

6. Goldstein, M. E., Wen-Jei Yang, and J. A. Clark, "Momentum and Heat Transfer in Laminar Flow of Gas with Liquid-Droplet Suspension Over a Circular Cylinder," *Transactions of the A. S. M. E.,* Vol. 89, Series C, No. 2, pp. 185-193, May, 1967.

7. Smith, J. E., *Heat Transfer Studies of Water-Spray Flows,* Northern Research and Engineering Corporation, ARL Report ARL 66-0091, Wright-Patterson AFB, Ohio, May, 1966.

8. Thomas, W. C., *Heat Transfer from a Wall Cooled by a Liquid Spray,* Ph. D. Thesis, Georgia Institute of Technology, Atlanta, Georgia, July, 1967.

9. Saterbak, R. T., *An Experimental Investigation of Heat Transfer from an Isothermal Cylinder Exposed to Two-Component Crossflow,* Master's Thesis, Georgia Institute of Technology, Atlanta, Georgia, June, 1967.

10. Pohlhausen, "Zur Naherungsweisen Integration der Differentialgleichung der Laminaren Reibungsschicht," *ZAMM,* Vol. I, pp. 252-268, 1921.

11. Mouradian, E. M. and J. E. Sunderland, "The Velocity and Temperature Distributions in a Liquid Film," *Applied Scientific Research*, Vol. 14, pp. 431-470, 1965.

12. Dyer, J. R., "Laminar Natural Convection from a Horizontal Cylinder with a Uniform Heat Flux," *Mechanical and Chemical Engineering Transactions (Australia)*, MC1, 1, pp. 125-134, May, 1965.

13. Roberts, Leonard, *A Theoretical Study of Stagnation-Point Ablation*, N.A.S.A. Technical Report R-9, 1959 (Supersedes NACA TN 4392).

14. Schlichting, H., *Boundary Layer Theory*, McGraw-Hill Company, Inc., New York, 1960, p. 153.

15. Kreith, Frank, *Principles of Heat Transfer*, International Textbook Company, Scranton, Pennsylvania, 1962.

16. Spiegel, M. R., *Applied Differential Equations*, Prentice-Hall, Inc., Englewood Cliffs, New Jersey, 1960, pp. 41-42.

17. Delavan Manufacturing Company, *Spray Droplet Technology*, Company Booklet, West Des Moines, Iowa, 1965.

18. Monsanto Chemical Company, Technical Bulletin I-180.

19. Dussourd, J. L., *A Theoretical and Experimental Investigation of a Deceleration Probe for Measurement of Several Properties of a Droplet-Laden Air Stream*, Ph.D. Thesis, M.I.T., Cambridge, Massachusetts, October, 1954.

20. Petrick, M. and B. S. Swanson, "Radiation Attentuation Method of Measuring Density of a Two-Phase Fluid," *The Review of Scientific Instruments*, Vol. 29, No. 12, pp. 1079-1086, December, 1958.

21. Alexander, L. G. and C. L. Coldren, "Droplet Transfer from Suspending Air to Duct Walls," *Industrial and Engineering Chemistry*, Vol. 43, No. 6, pp. 1325-1331, June, 1951.

22. Amstead, B. H., *On Techniques for Determining Liquid Droplet Concentrations in a High Velocity Airstream*, Master's Thesis, The University of Texas, Austin, Texas, 1949.

23. Jenkins, D. C., *The Acceleration of Water Drops by an Airstream of Constant Relative Velocity*, Aeronautical Research Council Paper No. C.P. 539, May, 1959.

24. Sucec, J., *On the Correction of the Reading Recorded by an Impact Tube Inserted into a Gas Stream Containing Entrained Liquid Particles*, Project Note NASA No. 9, Mechanical Engineering Department, The University of Connecticut, Storrs, Connecticut, August, 1963.

25. Brun, E. A., *Icing Problems and Recommended Solutions*, North Atlantic Treaty Organization, Advisory Group for Aeronautical Research and Development (AGARD), AGARDOGRAPH No. 16, 1957.

26. Brun, R. J., W. Lewis, P. J. Perkins, and J. S. Serafini, *Impingement of Cloud Droplets on a Cylinder and Procedure for Measuring Liquid-Water Content and Droplet Sizes in Supercooled Clouds by Rotating Multicylinder Method*, N.A.C.A. Report 1215, 1955.

27. Spalding, D. B., *Convective Mass Transfer*, McGraw-Hill Book Company, Inc., New York, 1963.

28. Levy, Solomon, "Integral Methods in Natural Convection Flow," *Transactions of the A.S.M.E.*, Vol. 77, Part 2, p. 515.

VITA

Jeffrey William Hodgson was born in Stockport, England on November 15, 1940. He came to the United States with his family in 1952 and became a naturalized citizen in 1959. After receiving his high school diploma from Lakeland (Florida) Senior High School in 1958, he entered Georgia Institute of Technology, where he received his Bachelor of Mechanical Engineering degree in 1963 and his Master of Science in Mechanical Engineering in 1965.

Mr. Hodgson is married to the former Margaret Hope Lind and they have two children.